1

Polymeric Electrode Materials in Modern Metal-ion Batteries

Zhenzhen Wu[1,*], Pan Yang[1,2,*], Shanqing Zhang[1], and Sheng Li[2]

[1]*Griffith University, School of Environment and Science, Gold Coast campus, Queensland 4222, Australia*
[2]*Nanjing Tech University, Key Laboratory of Flexible Electronics (KLOFE) & Institute of Advanced Materials (IAM), Nanjing 211800, China*

1.1 Introduction

In 1991, when Sony Corporation released the first commercial lithium-ion batteries (LIBs), the new era of portable smart electronic devices began. In the first generation of commercial LIBs, $LiCoO_2$ (LCO) and graphite were commonly used as cathodes and anodes, presenting a theoretical capacity of $274\,mAh\,g^{-1}$ and $372\,mAh\,g^{-1}$, respectively [1–3]. In order to further enhance the performance of LIBs, scientists have devoted a lot of effort and time to exploring inorganic electrode materials (IEMs), such as $LiFePO_4$ [4], $LiMn_2O_4$ [5], $LiNi^{II}_{1/3}Mn^{IV}_{1/3}Co^{III}_{1/3}O_2$ (NMC) [6] cathodes, and silicon anodes [7–11], over the next 30 years. IEMs were initially used in LIBs mainly because they have commercial accessibility and other significant merits as summarized in Table 1.1. IEMs can often be stable in organic electrolytes without noticeable structural and property changes, partly guaranteeing reasonable lifetimes. To date, three categories of general charge/discharge schemes for IEMs have been proposed and validated, including redox reactions, Li-ion intercalation/extraction, and alloying/dealloying at the cathode and anode [1, 12]. In addition, the raw materials, i.e. metal mines, are readily available for large-scale IEM production. Over the past 20 years, morphological science has promoted the production of a wide range of nanostructured IEMs, including 0D, 1D, 2D, and 3D nanomaterials and thus has driven the rapid development of IEMs [13–17]. However, current IEMs still have a series of weaknesses and limitations:

(1) The inherently rigid structures of IEMs could result in pulverization due to irreversible volume changes and significant phase transitions during charge/discharge, damaging the battery cycling life and even bringing in potential fire risk.

---

* Dr. Zhenzhen Wu and Mr. Pan Yang have equal contributions to this chapter.

Table 1.1 The comparison of characteristics and challenges between IEMs and PEMs.

Electrode materials		Advantages/characteristics	Challenges/issues
Inorganic electrode materials (IEMs)		• Low solubility in organic solvents • Established charge/discharge mechanism • Commercially available IEMs • Diverse morphologies of IEMs	• Rigid structure • Large volume fluctuation in charge/discharge • Irreversible phase transformation • Huge consumption of unsustainable earth sources and energy • Environmentally unfriendly in LIBs lifecycle
Organic electrode materials (OEMs)	**Single organic molecules electrode materials**	• Molecular tunability • Structural diversity and flexibility • Universal for accommodating monovalent and multivalent ions • Large electrons transfer number (up to over 20)	• High solubility in organic electrolytes • Poor electronic conductivity
	Polymeric electrode materials (PEMs)	• Less solubility in organic electrolyte • Sustainable resources on earth • Eco-friendliness • Low carbon footprints • Law price	• Vague charge/discharge mechanism • Poor electronic conductivity (apart from conducting polymers) • Thermal/Chemical/Electrochemical stability • Few morphologic of PEMs

(2) Large-scale production of IEMs is a high-carbon-footprint activity, consuming large amounts of unsustainable natural resources (e.g. lithium, cobalt, and nickel mines) at high temperatures. This will irreversibly pollute and damage the ecological environment.

(3) The limited natural resources on Earth cannot meet the almost unlimited demand for IEMs with the ever-increasing application of LIBs in electric vehicles and electrical grids.

The revolution and innovation of advanced energy storage devices in response to increasing economic costs and serious environmental pollution have driven the growth of a global green economy to meet carbon neutrality requirements worldwide. To this end, improving the battery performance and safety of LIBs is necessary, and most importantly, adopting sustainable electrode materials is critical in the design of the new generation of LIBs. Polymer electrode materials (PEMs) have tremendous potential to address these challenges and may play an important role in next-generation metal-ion batteries (MIBs), including LIBs, sodium-ion batteries (SIBs), potassium-ion batteries (PIBs), zinc-ion batteries (ZIBs), and aluminum-ion batteries (AIBs).

Similar to organic electrode materials (OEMs), PEMs are also composed of light, sustainable, and low-priced non-metallic elements such as C, H, O, N, and S, delivering various redox reactions and potentials to adopt current LIBs charge/discharge processes. As such, PEMs have a series of advantages over IEMs (see Table 1.1) [18].

(1) The production of most PEMs is a low-energy and low-carbon-footprint process as they can be refined from natural renewable sources, such as microorganisms, plants, and animal products.

(2) The deep-rooted relationship between battery properties (e.g. redox potential, current densities), redox groups, and functional groups (e.g. electron-donating or -attracting groups, electron-conducting groups) enables us to tune the energy storage mechanism of PEM-based LIBs, including output voltages, specific energy density, and power density. For example, in 2013, Morita et al. studied the voltage changes at different substituted groups on the TCNQ molecules, where $C \equiv N$ is the redox center [19]. The electron-donating group (e.g. methyl) enables the increase of the electronic cloud density around the $C \equiv N$ groups, making it easier to extract electrons on the redox center and thus reducing the voltage by c. 0.1 V. On the contrary, the electron-attracting group (e.g. fluorine atoms) presents the opposite effect, enhancing the voltage of TCNQ by circa 0.2 V.

(3) PEMs are suitable to produce flexible electrodes and devices because of their soft molecular backbones. For example, belt-shaped flexible batteries have been fabricated in collaboration with PEMs, showing good electrochemical performance [20, 21].

(4) PEMs are universal electrode materials, enabling the accommodation of the monovalent/multivalent metal ions, e.g. Li^+, Na^+, K^+, Zn^{2+}, Mg^{2+}, Ca^{2+}, and Al^{3+} [22].

In this chapter, we classify PEMs into two main categories according to the molecular structure and molecular weight (MW): (i) single organic molecules electrode materials (i.e. conventional OEMs), consisting of small and large organic molecules with small MW; (ii) PEMs, having repeating redox units in long chains with high MW. We adopt the theoretical molecular orbital theory of OEMs, i.e. the highest occupied molecular orbital (HOMO)/lowest unoccupied molecular orbital (LUMO) theory to simplify the theoretical discussion for PEMs. PEMs have long backbones and side chains decorated with numerous repeating redox units, presenting less dissolution and higher stability than single organic molecules. Considering the significant advantages of PEMs over OEMs in solubility, stability, and practical applications, we focus more on PEMs in this chapter.

Currently, PEMs still face several critical challenges in the course of their commercialization process (see Table 1.1). The chemical and electrochemical stability of PEMs in the existing organic electrolytes is a critical parameter affecting their adaptation to MIBs applications. The possible solubility of PEMs in organic electrolytes may significantly shorten the cycle time of the resulting LIBs. The electronic conductivity of PEMs (other than conducting polymers) must also be improved in electrode fabrication to fully use the redox sites during the charge/discharge process. Furthermore, due to the nature of polymerization reactions, the morphology of PEMs can be tuned in more complex ways than IEMs synthetic schemes. Therefore, PEMs have fewer morphology types than IEMs, and most PEMs are in powder or bulk forms. Finally, the general charge–discharge mechanism for PEMs will be systematically introduced based on the reaction of the redox groups.

This chapter reviews the categories, redox mechanisms, modification strategies, applications, and forward-looking perspectives of polymeric electrode materials in modern MIBs. The specific goals and actions of the design strategy are summarized as follows:

(i) Designing and controlling polymerization reaction to increase MW of PEMs to address PEM dissolution and stability issues.
(ii) Enhancing redox potential and energy density by employing suitable redox groups and functional groups in conjugated organic structures. The redox groups are the organic groups undergoing redox reactions and active ions insertion/extraction. The functional groups in the PEMs usually tune the redox potentials and structural stability.
(iii) Increasing the reactive sites to allow more electron transfer and store more ions.
(iv) Modifying the morphologic parameters (e.g. surface area and nanostructures) to accelerate ionic and electronic transportation in PEMs.

In this chapter, we will present a systematic and comprehensive understanding of PEMs to explore next-generation electrode materials with a high specific capacity, power density, and long cycle life.

1.2   Classification of PEMs

Generally speaking, six categories of PEMs (Figure 1.1, Table 1.2**)**, including organic carbonyls, organic sulfur (S) compounds, organic nitrogen (N) compounds, conducting polymers, organic radicals, and superlithiated compounds, are most popular in rechargeable MIBs [23–28]. They typically differ from each other because of their different redox groups.

   We also classify the PEMs according to the types of inserted ions: n-type PEMs undergo cations intercalation/extraction (e.g. Li^+, Na^+, K^+), p-type PEMs undergo anions intercalation/extraction (e.g. PF_6^-, ClO_4^-, BF^-, and $TFSI^-$), and bipolar-PEMs have both cation and anion reactions. The PEMs have different but tunable redox potentials, which are highly correlated with the potential output and energy density of the MIBs. The organic carbonyls, e.g. quinone, polyimide, pyrene 4,5,9,10-tetraone, cyclohexanehexone, deliver a voltage between 1.7 and
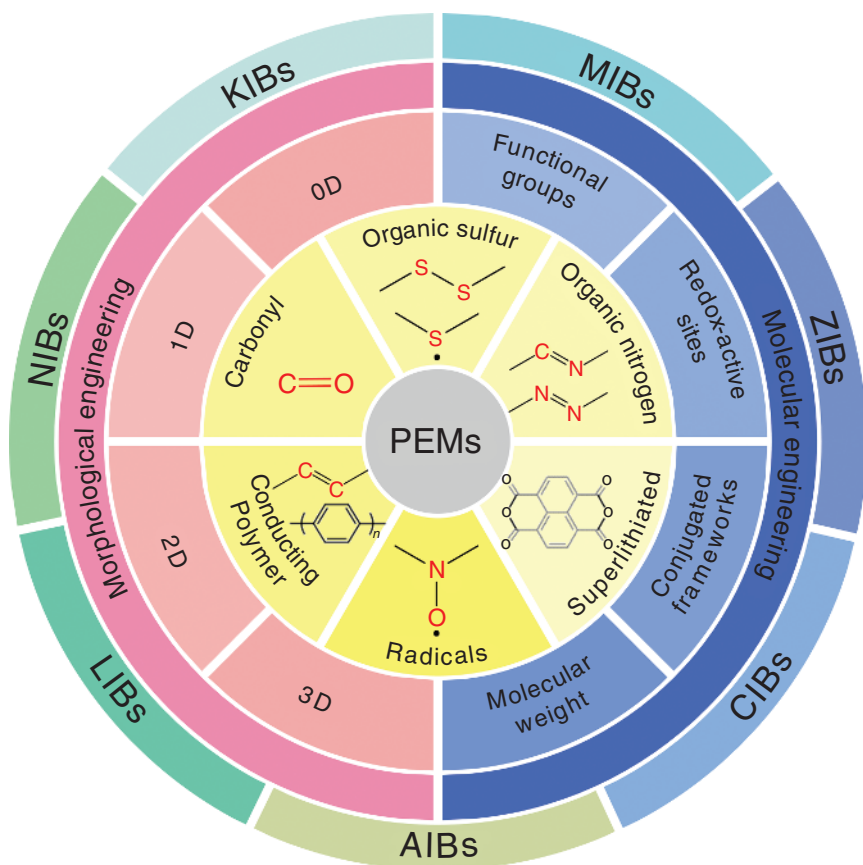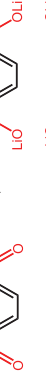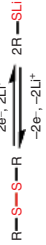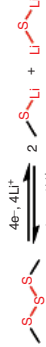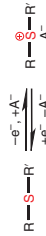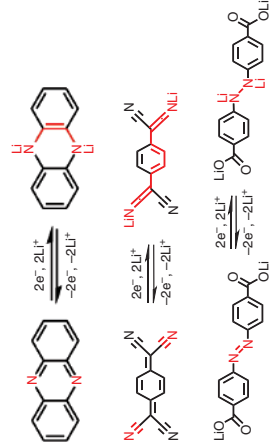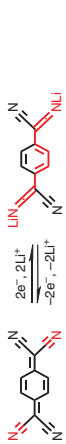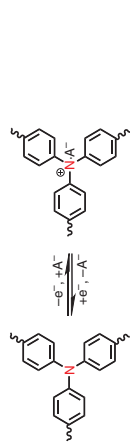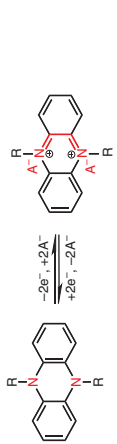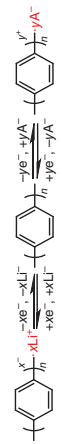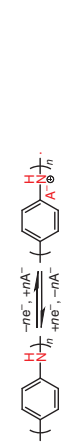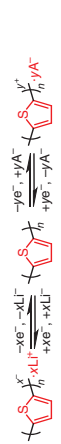

Figure 1.1   The classification and application of polymeric electrode materials (PEMs) in modern metal-ion batteries, according to chemical composition, morphology, and types of batteries.

Table 1.2 The classifications and (electro) chemical properties of PEMs.

Classification of PEMs (redox groups)	Types	Typical redox reaction scheme	Electro-organic chemistry	Features
1. Carbonyls (C=O)	Quinones		The addition of double bond	• High capacity • Moderate voltage plateau • High solubility • Low electronic conductivity
	Carboxylates			
	Anhydrides			
	Imides			
2. Organic sulfur compounds (—S—)	Disulfides		The cleavage/regeneration of single bond	• High capacity • Moderate voltage plateau • Poor cycling reversibility • Low electronic conductivity
	Polysulfides			
	Thioethers		Doping reaction	• Low capacity • High voltage plateau

3. Organic nitrogen compounds (—N—)	Imines		The addition of double bond	• High capacity • Low voltage plateau • Fast kinetics
	Cyano derivatives			• Moderate voltage plateau • High solubility
	Azo compounds			• High capacity • Low voltage plateau • High solubility
	Arylamine compounds		Doping reaction	• Low capacity • High voltage plateau • Fast kinetics • High electronic conductivity
			The addition of double bond	
4. Conducting polymers	Conjugated hydrocarbons		Doping reaction	• Low capacity • High and sloping voltage plateau • Fast kinetics • High electronic conductivity
	Conjugated benzene			
	Conjugated amines			
	Conjugated thioethers			

Table 1.2 (Continued)

Classification of PEMs (redox groups)	Types	Typical redox reaction scheme	Electro-organic chemistry	Features
5. Organic radicals	Nitroxyl radicals		Doping reaction	• Low capacity • Fast kinetics • Low electronic conductivity
	Dialkoxyaryl radicals			
	Galvinoxyl/ phenoxyl			
6. Superlithiated compounds	Redox active multi-functionals groups PEMs		The addition of double bond	• High capacity • Low voltage plateau

3.2 V (vs. Li/Li$^+$). Similarly, the organic S compounds (e.g. tetraethylthiuram disulfide) and organic N compounds (e.g. 7,7,8,8-tetracyanoquinodimethane, 5,6,11, 12,17,18-hexaazatri-naphthylene, the AZO compounds) show a working voltage between 1.55 and 3.0 V (vs. Li/Li$^+$). Interestingly, the p-type PEMs, such as conducting polymers and organic radicals, generally present a high working potential above 3.5 V (vs. Li/Li$^+$). For example, the conducting polymers, such as the polyacetylene (2.5–3.95 V vs. Li/Li+), polythiophene (3.0–4.3 V vs. Li/Li$^+$), polyaniline (2.5–4.01 V vs. Li/Li$^+$), and polypyrrole (2.0–3.5 V vs. Li/Li$^+$), are used as high-voltage PEMs cathodes. Organic radicals, such as poly (2,2,6,6-tetramethylpiperidinyloxy methacrylate) (PTMA) with 2,6,6-tetramethyl-1-piperidinyloxy (TEMPO) redox radical sites, have a high potential plateau (c. 3.6 V, vs. Li/Li$^+$). Another voltage range of PTMA radicals is obtained at circa 2.5–3.2 V (vs. Li/Li$^+$) at the enhanced electronic conductivity networks. In contrast, the superlithiated PEMs, such as 1,4,5,8-naphthalenetetracarboxylic dianhydride, polyazaacene analog, the imine-based COFs, multi carbonyl polyimides, and polyimide Schiff base, have anodic voltage plateaus between 0 and 1.6 V (vs. Li/Li$^+$).

1.2.1 Carbonyls

The first carbonyl compound, i.e. dichloroisocyanuric acid, was reported in 1969 and exhibited high electrochemical activity for storing Li ions, but lacked capacity stability [29]. Since then, carbonyl compounds have been extensively studied in the electrochemical energy field due to their high theoretical specific capacity (up to 957 mAh g^{-1} per C=O groups), high battery reversibility, and structural tunability [30–38]. The carbonyl group, which undergoes double bond addition in the battery process, is significant in deciding the energy density and electrochemical activity of the PEMs. In the discharge process, the C=O double bond is added by electrons, transformed into the C—O single bond, and bonded with Li$^+$ cation, presenting medium voltage.

  As shown in Table 1.2, carbonyl compounds can be divided into quinones, carboxylates, imides, and anhydrides. (i) The quinones, two C=O groups located in the hexagonal cyclic diketone structure, are extensively studied as the typical carbonyl compounds. For example, 1,4-benzoquinone (BQ) molecule is able to accept two electrons and two Li$^+$ ions to achieve a high theoretical capacity of 496 mAh g^{-1} [39, 40]. Specifically, the cyclohexanehexone (C$_6$O$_6$) owns six C=O groups in a six-membered ring, supplying the highest theoretical capacity (957 mAh g^{-1}) among all organic carbonyls (Figure 1.2a) [32]. An ultrahigh practical capacity and cycling stability were also obtained at the low current density between 1 and 4 V (vs. Li/Li$^+$) (Figure 1.2b,c) [32]. This specific carbonyl molecule reveals the great potential of carbonyl PEMs in high-energy battery systems. (ii) The carboxylates consist of the aromatic ring(s) and carboxylate groups (e.g. —COOLi). The carboxylate groups donate electrons to the carbonyl groups, reducing the operation potentials of the whole molecules. This is why carboxylates are normally used as anode materials [38, 41–43]. (iii) Imides are made of —(C=O)—(N-R)—(C=O)—, where the N atom is bonded to two carbonyl groups attached to the aromatic ring structure. Imides
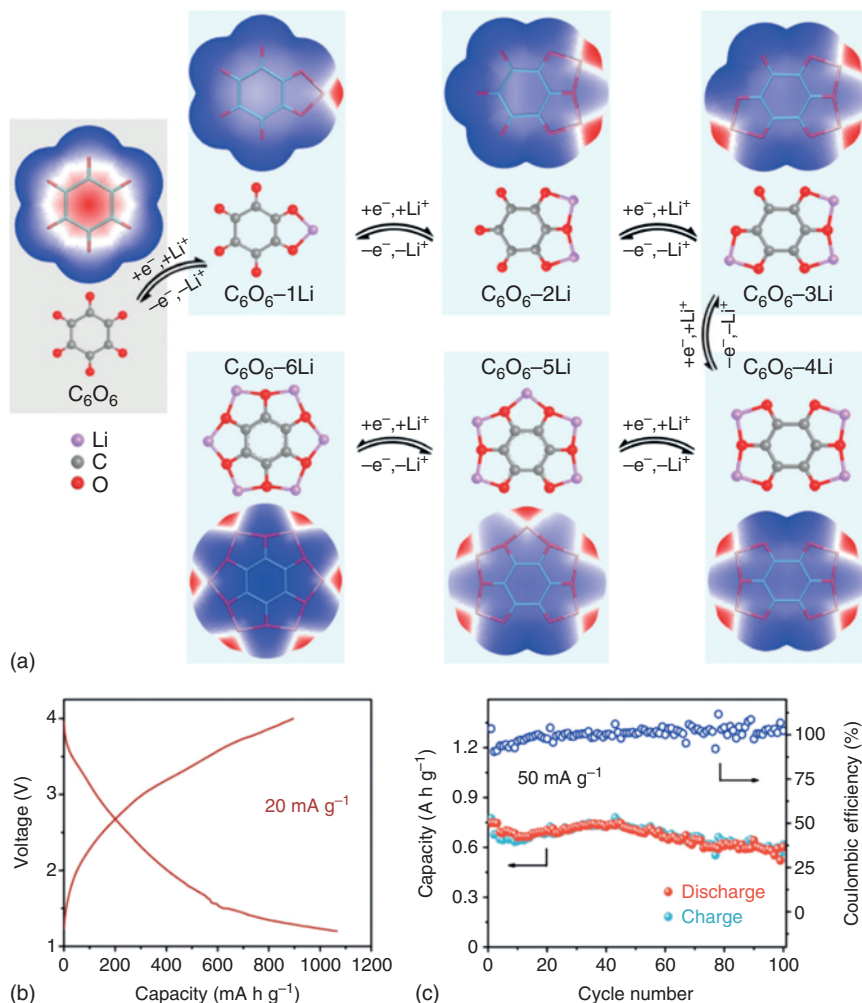
Figure 1.2 Electrochemical performance and mechanism of organic carbonyls, e.g. C_6O_6, in LIBs. Source: Reproduced with permission from Ref. [32]. Copyright 2019, Wiley-VCH Verlag GmbH &Co. KGaA, Weinheim.

can allow three main reactions, including enolate reaction of C=O groups, the association/dissociation of cations with active O atoms, the interactions between the anions at the N atoms [44, 45]. (iv) Anhydrides composed of anhydrides with large conjugated structures could deliver excellent structural and cycling stability [46–48].

However, carbonyl compounds, especially carbonyl compounds with low molecular weight, present serious dissolution problems in aprotic electrolytes due to their interaction with electrolyte solvents [31, 49, 50]. Although carbonyl compounds have low solubility in aqueous solvents, their discharge products can be dissolved in aqueous electrolytes. In addition, their low electronic conductivity restricts fast

ions transportation. These drawbacks limit carbonyl compounds in low cycling life and low power capacity.

1.2.2 Organosulfur

The organic sulfur PEMs are defined as organic compounds with redox-active S atoms, including disulfides, polysulfides, and thioethers (Table 1.2). They are low cost, environmentally friendly, and biodegradable. Unlike the C–S bond, the S–S bond has a longer bond length and smaller bond energy. That is why the disulfides and polysulfides tend to reversibly break and regenerate the S–S bonds with two electrons transferring [51–53]. In contrast, the thioethers present quite different redox mechanisms due to the S atom delivering a large atomic radius and less binding force for the outer electrons in the nucleus. In the discharge process, the thioether reversibly transforms between C–S–C and C–S$^+$–C and interacts with the active anions at a relatively high voltage. Thioethers deliver better cycling stability than disulfides and polysulfides because there are no S–S bonds breakage and reformations. The thioethers also have faster electronic conduction due to the lone pair of electrons on S atoms having π-electron delocalization with the aromatic rings.

In 1988, Visco et al. reported the first organic sulfur PEMs [54]. Since then, ever-increasing efforts have been devoted to cultivating organosulfur compounds to store the active ions. In order to address the dissolution issues of organodisulfides, Wang et al. applied different N-containing heterocycles in the disulfides molecules (Figure 1.3a) [55]. DFT calculation reveals that the 2,2′-DpyDS presents the highest energy gap between the LUMO and HOMO (Figure 1.3b). The 2,2′-dipyridyl disulfide (2,2′-DpyDS) delivers a long cycling life of up to 500 cycles, because the N/Li/S bridges coordinate with each other and thus suppress the dissolution of their discharge products (Figure 1.3c,d). Thioethers usually go through "thioether–sulfoxide–sulfone," enabling a high specific capacity of around 500–800 mAh g^{-1}. Based on the study of this series of disulfide molecules, it was found that the chemical environment of organic S PEMs is quite significant to determine their cycling performance and specific capacity.

Similar to other PEMs, organic S compounds also suffer from poor electronic conductivity and sluggish kinetics during the energy storage process. The S–S bond in the main chains is preferred because of the low solubility. In contrast, the side chains bonded with S–S bonds are not conducive to long cycling because of the low re-bonding efficiencies in the charging process. Thus, it has been suggested to load the S–S bonds in the side of the same chains to increase Coulombic efficiency [56].

1.2.3 Organic Nitrogen (N)

In general, reversible electrochemical reactions are more likely to occur in two chemical environments. One is a conjugated molecular structure, which can facilitate electron transportation in the electrochemical reactions and charge delocalization of discharge products. Another is heteroatoms-bonded structure (e.g. O, S, and N) accompanied by a pair of lone electrons, which confer a high redox
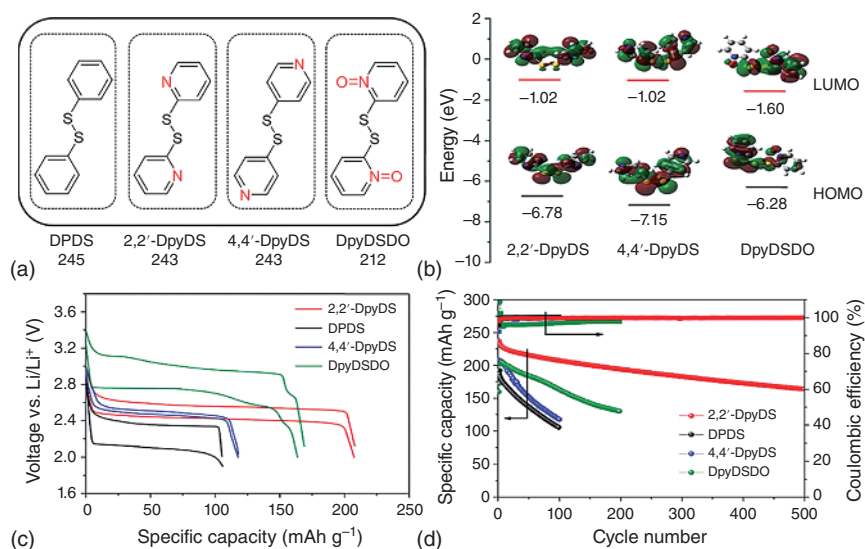
Figure 1.3 The electrochemical properties of organic sulfur (S) compounds. (a) S–S bonds in different chemical environments, (b) calculated LUMO and HOMO value, (c) the charge–discharge profiles in the 100th cycle, (d) the cycling performance at 0.5 C rate. Source: Reproduced with permission from Ref. [55]. Copyright 2019, the Royal Society of Chemistry.

activity and increase the electronic conductivity of the whole structure [57–59]. Both design criteria are usually considered to conceive high-performance PEMs. Generally speaking, the N heteroatoms containing PEM have two kinds of reactions mechanisms, which are determined by their different bonding environment. First, addition of N contained double bonds (e.g. imine group of N=C bonds, cyano groups of N≡C bonds, azo groups of N=N bonds) into a single bond and then interaction with the active anions. In this redox reaction, no breakage of N—C/N—N/N—O single bonds occurs because of the strong bonding effect between the N atoms and adjacent atoms, resulting in good electronic reversibility. The second is anion adsorption in the active N atoms loaded in the saturated amines of arylamine groups. This kind of N atom prefers to lose one electron and then react with the anions [27].

Imine compounds, bonding with N=C double bond, tend to convert into N—C single bond associated with one or multi electrons transfer through the inter-molecules [60, 61]. Typically, the C=N redox centers in the aromatic groups, except for strongly electron-deficient groups (e.g. pyrazine rings), and shows a wide range of working potentials. For example, hexaazatrinaphthalene (HATN), owning six C=N groups per unit, undergoes six-electron reactions between 1.2 and 3.9 V (vs. Li/Li$^+$) [58, 59]. Their voltage platform occurs around 1.5 and 2.5 V (vs. Li/Li$^+$). After polymerization, the P-HATN presents excellent cycling stability of up to 10 000 cycles, a high specific capacity of around 450 mA h g^{-1}, and an enhanced power density of 20 °C [62]. Specifically, the imine includes pyrazinyl compounds,

triazinyl compounds, Schiff bases, and pteridine derivatives. The pyrazinyl and triazinyl compounds usually work at the $1 \sim 2$ V (vs. Li/Li$^+$) with the cation insertions, rarely at the relatively higher redox potential with the anion interactions [63]. Schiff bases, i.e. R_1—N=CH—R_2 where R_1, R_2 are aromatic groups (Ar), conduct two-electron transfer reactions as the potential anode at around 1 V (vs. Li/Li$^+$). In the polymerized Schiff bases, the inactive Ar aromatic groups significantly boost the stability of the whole structure during the long cycling life [60, 64]. Pteridine derivatives possess conjugated diazadiene moieties that facilitate the biological redox reactions accompanied by the proton-coupled electron transfer at the N atoms [65].

Cyano compounds, composed of N $\equiv$ C bonds, were firstly reported in LIBs in 1984 [66]. The 7,7,8,8-Tetracyanoquinodimethane (TCNQ) is the presentive cyano derivative, involving 2-electrons transfer reactions from TNCQ to TNCQ^{2-} at relatively high working potential around 3.0 V. Their structure irreversibly composes and forms LiCN below 1.0 V. In particular, the cyanide groups decorating the aromatic rings of cyano compounds enable decrease of their working potential to around $1.0 \sim 2.0$ V [67].

Azo compounds, where the N=N double bonds are the redox-active centers, were firstly reported in 2018 [68, 69]. The N=N double bonds tend to be added to by two electrons, then transform into N—N single bond, and interact with two cations. When the Azo groups connect with phenyl groups, their redox potential can decrease to 1.5 V (vs. Li$^+$/Li). However, a lower potential may damage their structure.

Arylamine compounds, where N atoms act as the redox-active centers to insert the anions, are the typical N-based cathode materials. The N atoms in such a chemical environment could donate the electrons and simultaneously react with the anions (e.g. PF$_6{}^-$) [70, 71]. Take the poly(triphenylamine) (PTPAn) as an example, the nonplanar structure of the triphenylamine group enables localization of positive charges in the oxidized state of N atoms. As a result, the N atoms lose one electron and convert into N$^+$ to incorporate with PF$_6{}^-$ anion [72].

1.2.4 Conducting Polymers

Conducting polymers are an attractive class of conjugated PEMs, with high electronic conductivity and structural stability. In 1981, polyacetylene was the first example of conducting polymers reported as the cathode in LIBs [73]. Conducting polymers have four major categories based on the different electroactive redox groups: (i) conjugated hydrocarbons such as polyacetylene with the electronic conductivity of around 10^{-5} S cm^{-1}, (ii) conjugated benzene such as polyparaphenylene with around 10^{-3}–10^{-4} S cm^{-1}, (iii) conjugated amines such as polyaniline and polypyrrole with around 10^{-2}–10^{-4} S cm^{-1}, and (iv) conjugated thioethers such as polythiophene with 100 S cm^{-1} (Figure 1.4a) [23, 25, 28, 57].

Generally, the electron dislocation in the conjugated structure allows both the acceptance and donation of electrons (i.e. bipolar-type reactions). In most circumstances, the conducting polymers (e.g. polyaniline, polypyrrole, and polythiophene) tend to be more stable in the oxidized states than in the reduced states because of

Polypyrrole (PPy)

Polyaniline (PANI)

Polypthiophene (PTh)

Poly(3,4-ethylenedioxythiophene) (PEDOT)

(a)

(b)
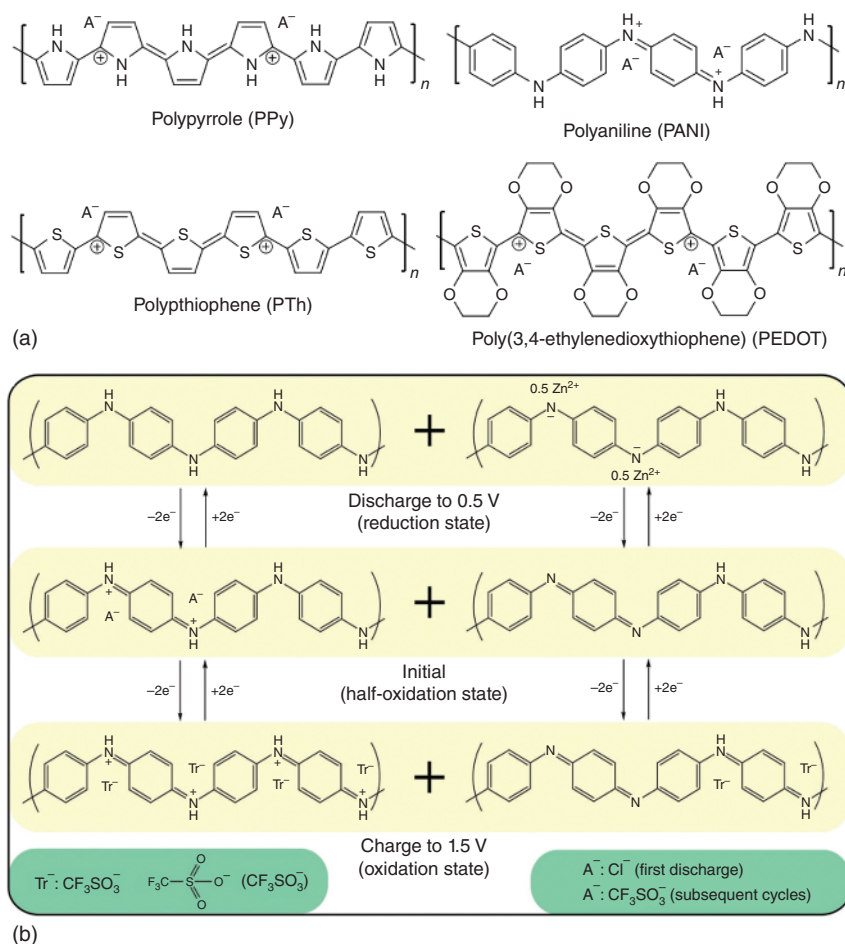
Figure 1.4 (a) Four types of typical conducting polymers. Source: Reproduced with permission from Ref. [74]. Copyright 2019, American Chemical Society. (b) The redox mechanism of polyaniline. Source: Reproduced with permission from Ref. [75]. Copyright 2018, WILEY-VCH VERLAG GMBH & CO. KGAA, WEINHEIM.

their electron-rich properties. Their working voltage is as high as $2.5 \sim 4.5\,\text{V}$ (vs. Li/Li^+) [74, 76–78]. Polyaniline (PANI) has been developed as a cathode in the aqueous zinc ions battery. The PANI cathode delivers outstanding power density and cycling stability because of the hybrid mechanism (Figure 1.4b) [75]. Nitrogen atoms in PANI are doped ($=NH^+$—) and undoped ($=N$—) forms because they are dominantly in the half-oxidation state. During the first discharge, the doped nitrogens are reduced, and simultaneously, the Cl^- ions get off the PANI framework [75]. Then, the -NH- moiety is further reduced to $—N^-$- and reacts with Zn^{2+} ions. As a result, it delivers a high capacity of c. $95\,\text{mAh}\,\text{g}^{-1}$ at the high rate of $5\,\text{A}\,\text{g}^{-1}$, which is around 47.5% at $0.05\,\text{A}\,\text{g}^{-1}$. The high capacity of $191\,\text{mAh}\,\text{g}^{-1}$ is obtained again when the cycling comes back to the $0.05\,\text{A}\,\text{g}^{-1}$ [75]. In other cases, some conducting polymers

(e.g. polyacetylene and polyparaphenylene) are subject to both cations and anions insertion [79]. They are suitable for high-voltage cathodes in hybrid batteries with a relatively high specific capacity.

However, the conducting polymers still suffer from drawbacks, including low discharge capacity, sloping voltage platform, and self-discharge. Theoretically, the capacity of conducting polymers is decided by the ions doping degree and the active anions. The high degree of doping in the conducting polymers allows for high specific capacity. However, the highly doped structures cause serious charge repulsion interactions between the neighbor units, increasing the inactive sites and reducing the reversibility. For example, the polyacetylene cathode provides a CE of 65.6% at a doping level of 0.097, but 35.5% at 0.194. After optimization, the relatively low doping degree of circa 0.3–0.5 is the preferred structure. Of course, the capacity in such a low doping degree is insufficient. Furthermore, their electrochemical working potential exhibits a sloping tendency since the vibrant doping degree continuously changes the equilibrium potential during the reaction process. What is more, anionic dopants gradually dissociate from the conducting polymers structures during long-term cycling, causing self-discharge issues.

1.2.5 Organic Radicals

Radical polymers are full of pendant redox-active groups in addition to the polymeric main chains, exhibiting high power density and long cycling life. They have dense unpaired electrons, facilitating the slight structural changes and electron rearrangements during the reactions. The poly(2,2,6,6-tetramethylpiperidinyl-1-oxy-4-methacrylate), abbreviated as PTMA, was the first reported radical polymer used as the cathode (Figure 1.5a) [80]. In the charging process, the nitroxyl radicals oxidize into cations, interact with the active anions, and generate oxoammonium salts. A reverse reduction reaction occurs in the charging process [80]. The PTMA delivers obvious charge/discharge plateau at around 3.5 V (vs. Li/Li$^+$) both at 0.1 and 1.0 mA cm^{-2} (Figure 1.5b) [80]. Radical polymeric electrodes present excellent power density and slight voltage polarization, attributed to the outer electron self-exchanging reaction at the neighboring radical groups [81]. However, the
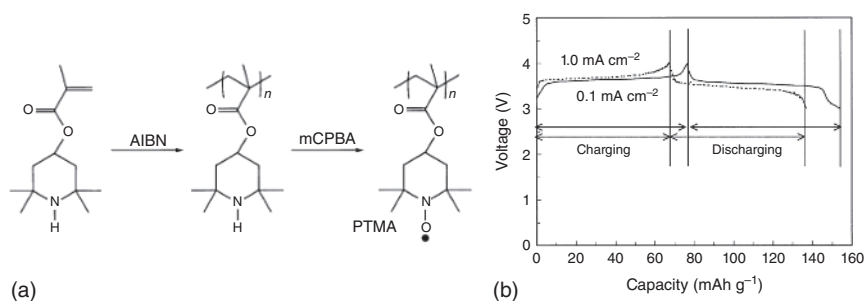

Figure 1.5 The (a) typical radical-based PEMs and (b) corresponding charge–discharge curves. Source: Reproduced with permission from Ref. [80]. Copyright 2002, Elsevier Science B.V.

specific capacity of radical polymers is normally restricted below $150 \, \text{mAh g}^{-1}$ due to the inherent single-electron transfer reaction and large molecular weight. Furthermore, the low conductivity of radical polymers usually requires a high proportion of conductive additives to ensure quick electron transfer within electrodes, which inevitably imposes further constraints on their overall specific capacity [82].

1.2.6 Superlithiated Compounds

Despite the structural diversity and different electrochemical redox-active centers, most PEMs fail to provide practical capacities beyond $400 \, \text{mAh g}^{-1}$, making them insufficient to compete with the practical IEMs [83]. There are many inactive moieties on PEMs that take up extra weight and reduce overall capacity. Fortunately, multifunctional superlithiated compounds own many sites capable of reverse lithiation at the unsaturated C=C/C≡C bonds and other active groups [24, 84–91]. The overlithiation reaction can greatly facilitate electron transfer and achieve an exciting 1 : 1 Li/C ratio, corresponding to a theoretical maximum specific capacity of approximately $2232 \, \text{mAh g}^{-1}$. For example, a covalent organic framework (COF) based on 1,4–diaminobenzene and 1,3,5-benzenetricarboxaldehyde was anchored with the CNTs to prepare COF@CNTs composites (Figure 1.6) [85]. This special composite exhibits a 14-electrons transfer reaction per unit at 2 C=N groups and the unsaturated C6 rings [85]. The different free energies (ΔG) at four stages inspire the superlithiation reactions on COFs (Figure 1.6a) [85]. Accordingly, the COF presents a high specific capacity of $1536 \, \text{mAh g}^{-1}$ at $100 \, \text{mA g}^{-1}$ (Figure 1.6b) [85].

Despite the high energy density, superlithiated PEMs still face some challenges. The overlithiation process may disrupt the crystal structure, resulting in poor cycling performance and low initial CE. Furthermore, the overlithiation process inevitably destroys the π-conjugated structure and reduces the electronic conductivity, increasing the electrochemical polarization and reducing the battery life.
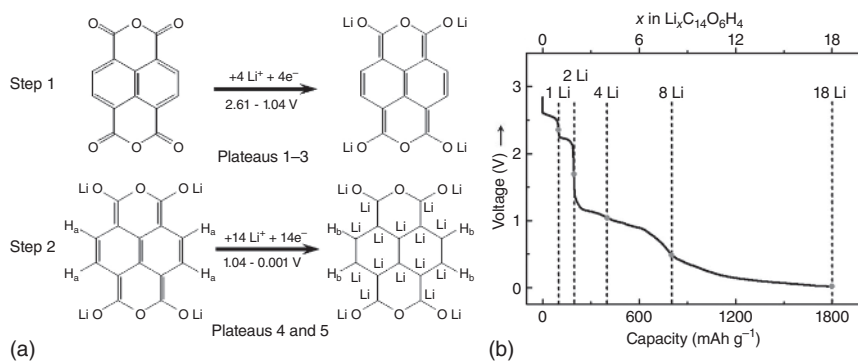
Figure 1.6 The (a) reactions mechanism and (b) discharge profiles of typical superlithiated compounds (e.g. NTCDA). Source: Reproduced with permission from Ref. [85]. Copyright 2012, WILEY-VCH Verlag GmbH & Co. KGaA, Weinheim.

1.3   Molecular Engineering of PEMs

In-depth investigation of PEMs in battery systems demonstrates how they face severe challenges such as low voltage output, low practical capacity, and poor cycling performance. These mainly come from their molecular-level drawbacks, such as limited ionic conduction, inherent insulation, and high solubility, in the aprotic electrolytes. Fortunately, some effective strategies have been proposed to tune the molecular structures of PEMs to fundamentally overcome the above issues. These strategies are originally based on the functional groups, the redox groups, the polymeric chains, and the (non)conjugated backbone (Figure 1.7). In this section, we present the significant electrochemical parameters: specific energy density (e.g. voltage output, electron transfer quantity, specific capacity), power density (e.g. reactions kinetics), and cycle performance (e.g. chemical/structural stability).

1.3.1   Specific Energy Density

Specific energy density is a critical indicator to evaluate the battery performance of energy storage devices. Two equations significantly correlate with the specific energy density (E).

First:

$$E = V \times C \tag{1.1}$$

where V is the working voltage and C is the theoretical specific capacity.

Second:

$$C = nF/3.6 \ \ \text{MW} \tag{1.2}$$
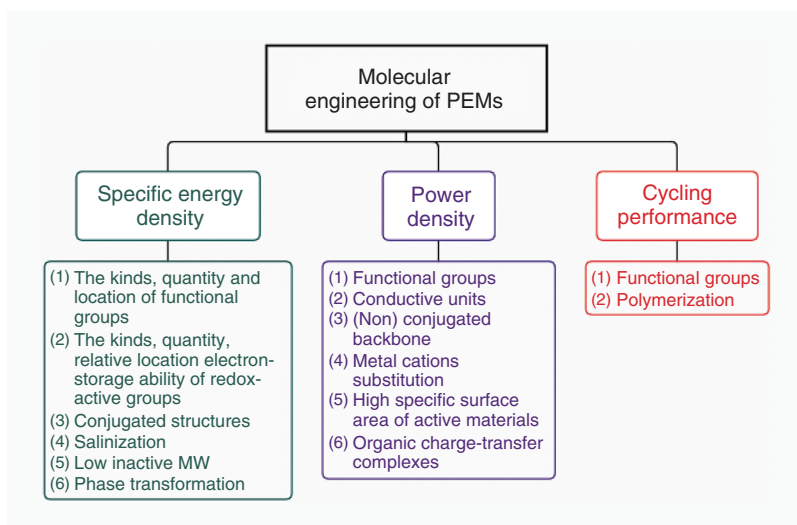
Figure 1.7   The molecular engineering of PEMs to enhance electrochemical performance, such as specific energy density, power density, and cycling performance.

where n is the number of transfer electrons, F is the Faraday constant, and MW is PEMs molecular weight per unit. Accordingly, the specific energy density will systematically be introduced according to the voltage output, electron transfer quantity, and specific capacity.

The working voltage, which is the positive voltage minus the negative voltage, critically decides the whole energy density of the battery. In other words, increasing/decreasing the potential of polymeric cathodes/anodes can increase the energy density of the batteries. PEMs in anions insertion, such as the conducting polymers and organic radicals, inherently obtain a high redox potential of around 3.5 V (vs. Li/Li$^+$). However, the PEMs in cations insertion, such as organic carbonyls and disulfides, usually undergo the redox reactions at a relatively low potential below 3.0 V (vs. Li/Li$^+$), which is too high for the anode. Thus, more research effort has focused on the voltage modification of cation-inserted PEMs.

The redox potential of the PEMs is decided by the molecular orbital energy and the electron cloud of materials [92]. In other words, functional groups with electron-withdrawing/donating properties at the molecular level are an effective way to tune the redox potential of the PEMs (Figure 1.8). Specifically, electron-withdrawing groups, such as halogen groups [19, 94–98], cyano groups [98–100], sulfonyl groups [101, 102], and heteroaryl groups [103–105], enable
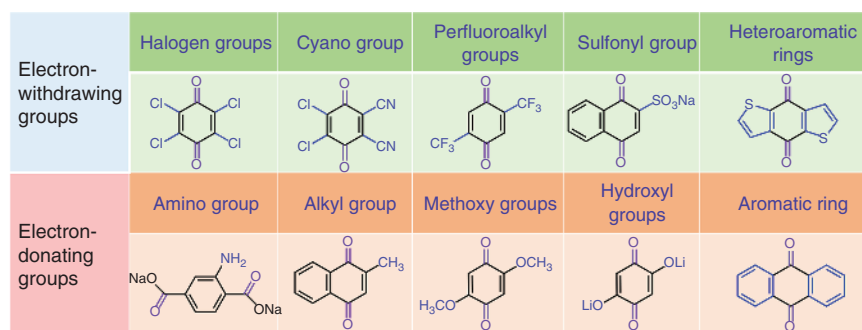
(a)
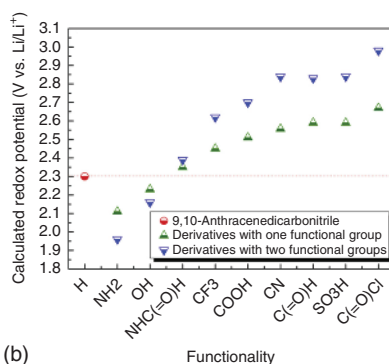
(b)

Figure 1.8 (a) Typical functional groups (i.e. electron-withdrawing/donating groups) in potential tuning. (b) The potential of 9,10-anthracenedicarbonitrile-derived materials with different functional groups. Source: Reproduced with permission from Ref. [93]. Copyright 2019, Elsevier Science B.V.

tuning of the LUMO and enhance the redox potential. The redox potential linearly correlates with the LUMO energy (i.e. reduction energy of the molecules) [104, 105]. Of course, the redox structures inherently present different distributions of electron clouds, and thus, different molecules conform to different linear correlations. For example, halogen groups have relatively high electronegativity, i.e. huge electron affinity, which will have electron-withdrawing effects on the electron cloud of the redox centers, lowering the LUMO energy level [98]. Therefore, a higher redox potential is required for the redox-active center to provide electrons. Moreover, the electron-deficient/rich aromatic rings also can tune the molecular orbital energy. For example, replacing the aromatic carbon atoms via electronegative heteroatoms (e.g. N, S, O) leads to inhomogeneity in electron delocalization, leading to negative charge toward these electron-withdrawing heteroatoms transfer [106]. In contrast, electron-donating groups (e.g. amino group, alkyl groups, methoxy group, –OLi/Na) are necessary to reduce the potential because they can provide extra electron clouds to the redox centers and increase the LUMO energy level of the PEMs [19, 107, 108]. This is very important when constructing the anode PEMs.

Conjugated structures tend to improve the delocalization of the electrons via π–π orbital interaction and the resonance effect. This can be applied by extending the conjugation length, relocating the conjugation units, and using different conjugated frameworks [19]. Salinization, i.e. cation substitution (e.g. Mg^{2+}, Ca^{2+}, and Ba^{2+}), also can tune the redox potential of PEMs, especially carboxyphenolate-based materials [35]. After the substitution, the host structure can modulate the inductive effects, e.g. electronic charge perturbation, of the active skeleton.

Electron transfer quantity is directly correlated with the types, quantity, and electron-storage ability of redox-active groups. BQ with two C=O active groups owns a theoretical capacity of $496 \, mAh \, g^{-1}$, while cyclohexanehexone with six C=O groups presents a high capacity of $957 \, mAh \, g^{-1}$ [32]. Increasing the electron-accommodating capability of redox centers via replacement of the O atoms by S atoms in the carboxylate groups is a successful example [109]. That is because the sulfur-substituted structure owns a higher electron density, which improves electron dislocations, thereby facilitating electron transfer.

The specific energy density of a battery is also related to the specific capacity involving the MW of the molecule chains or repeating units. Although grafting redox functional groups (such as halogen groups and alkyl groups) and conjugated moieties can increase the amount and ability of redox-active centers, it still leads to an increase in molecular weight and thus inevitably compromises its theoretical specific capacity [40]. In contrast to the theoretical specific capacity, the practical specific capacity also relates to the phase transformation, materials morphology, and the ionic/electronic conductivity of the electrode. For example, $Na_2C_6O_6$ occurs during irreversible phase transformation from α-state to γ-state [36].

1.3.2 Power Density

Power density comprehensively evaluates the electrochemical performance of a battery system, which depends not only on the output voltage but also on the power density. In practical applications, the energy capacity needs to be charged to 80%

within 15 minutes [110], meaning that a high rate capacity is significant for electrode materials. However, PEMs generally suffer from some inherent drawbacks, such as low electronic conductivity (especially for small MW PEMs), which limits their power density. The high electrical conductivity, fast redox kinetics, and small active particle size are critical to high-power-density PEMs.

In order to enhance the power density, many strategies have been reported: (i) The power density is largely determined by their intrinsic conductivity, which relates to the band gap between the LUMO and HOMO energy levels. As mentioned above, functional groups feasibly tune molecular orbital energy levels. A new naphthoquinone (NQ) derivative (i.e. 2,3-diamino-1,4-Naphthoquinone, DANQ) was synthesized by simple molecular substitution of amino groups at the NQ ring [111]. Most quinones have a wide band gap of around 4.0 eV, while DANQ molecule has a very low value of 2.7 eV, which is like semiconductors. This is due to the strong electron-donating effect of amino groups to the NQ rings, which destabilize the HOMO energy and hence reduce the HOMO–LUMO gap. The low band gap of DANQ facilitates the high lithium ions and electrons diffusion rate in the cathode. After the modification, the DANQ cathode delivers a high specific capacity of $250 \, mAh \, g^{-1}$ and discharge potential plateaus between 2.3 and 2.5 V, and 99% capacity attention after 500 cycles at 0.2 °C. (ii) The addition of conductive units can effectively promote electron transfer inside the active structure, thereby enhancing the high power density. Yao et al. firstly reported a "π-conjugated redox polymer" via the integration of π-conjugated backbones and the redox-active sites. This organic structure can be reversibly n-doped to a high doping level of 2.0 and high electronic conductivity [112]. Experiment shows a high-rate capability of this as-prepared structure, which takes 72 seconds per charge–discharge cycle and 96% capacity retention after 3000 cycles. (iii) π-Conjugated structures can rearrange the electron clouds in PEMs. Extending the π-conjugated structure enables enhanced intermolecular interactions (e.g. C–H π–π interactions) and thus increases electron-transfer kinetics. A conjugated copolymer is designed with phenothiazine redox-active groups and bithiophene monomers [113]. The π-conjugated structure makes the copolymers with semiconducting nature. At the high rate of 100 °C, the capacity of 30 000 cycle is 97% of the first cycle. (iv) Non-conjugated linkages are also important. It was reported that non-conjugated bonds, such as carbonyl groups, can specifically facilitate Na^+ adsorption, leading to excellent rate performance in Na-ion batteries [114]. A non-conjugated carbonyl group on the polyimides (Poly[PDI]s) was used as the example. For the non-conjugated diketones linked polymer, an enhanced rate performance ($2 \, A \, g^{-1}$) and cycle stability (the small capacity decay rate of $0.0039 \, mA \, h \, g^{-1}$/cycle) were obtained. (v) The substitution of metal cations is also effective. For example, the replacement of Ag^+ with the Li^+ ions in lithium terephthalate (Li_2TP) can form Ag_2TP, which is used as anode in the sodium-ion battery [115]. The Ag_2TP can *in situ* generate conductive Ag nanoparticles on the electroactive sites (i.e. terephthalate moiety) after the cycles due to the relatively high redox potential of 0.799 V (Ag^+/Ag, vs. standard hydrogen electrode). The resulting metallic Ag particles improve the electronic conductivity on the electrode materials surfaces. (vi) The increased surface area favors the

contact area between the active material and the electrolyte and promotes ion transfer kinetics. A series of microporous PEMs (e.g. SPTPA, YPTPA, OPTPA) were prepared based on the triphenylamine (TPA) segments [70]. They have the same theoretical capacity because of the same redox segments (TPA). But their surface areas vary depending on the polymerization method. The surface area of SPTPA and YPTPA can achieve 544 and 1557 $m^2 g^{-1}$, respectively. In contrast, the OPTPA presents a low surface area of 66 $m^2 g^{-1}$. As for the battery test, the YPTPA shows a high-rate capability of 97.6 mAh g^{-1} in less than three minutes at the high current density of 2 A g^{-1}. However, the OPTPA only has 48.2 mAh g^{-1} at the same testing parameters. (vii) The addition of conductive carbon has been widely used in the PEMs preparation process to enhance electron conduction and suppress the PEMs dissolution. But the external carbonaceous materials can increase the mass of inactive materials on the electrode, and this reduces the volumetric and mass energy density.

1.3.3 Cycle Performance

Service life is an important parameter for evaluating the overall performance of a battery in practical applications. However, the cycling performance of PEMs, especially small MW PEMs, suffers from inherent solubility in electrolytes. Therefore, overcoming the challenge of solubility has always been regarded as one of the hotspots of PEM manufacture. In addition, insufficient reversibility, volume changes, and structural changes are also potential factors deciding cycling performance.

To improve cycling performance, different molecular engineering strategies were used to address the above problems: (i) Changing the polarity similarity helps suppress solubility. Some functional groups (—COOLi, —COOK, —SO$_3$Na, —OLi, —Ona), with high polarity can enhance molecular polarity and thus restrict their solubility. It should be noted that these functional groups should not strongly influence the voltage plateau of the resulted PEMs. For example, two lithiooxycarbonyl (—CO$_2$Li) groups were connected to the p- and o- quinones [116]. Different from the parent PEMs, the —CO$_2$Li modified PEMs present excellent cycling performance on the cathode part. The modified PEMs do not have significantly different redox potential from the parent PEMs due to the Hammett value of σ_p and σ_m for —CO$_2^-$ being 0.11 and 0.02, respectively. (ii) Introducing heteroatoms (e.g. ortho-N atoms) in the phenyl rings can greatly tune the solubility [55]. This strategy is especially effective for the organodisulfides, where a redox reaction occurs when breaking and regeneration of the S–S bonds. Their discharged product is soluble in the electrolytes and thus suffer from serious capacity decay during cycling. Three disulfides with various N-containing heterocycles were prepared; those are 2,2′-dipyridyl disulfide (named as 2,2′-DpyDS), 4,4′-dipyridyl disulfide (abbreviated as 4,4′-DpyDS), and 2,2′-dipyridyl disulfide-N,N′-dioxide (called as DpyDSDO). The N atom in the structure is an electron-withdrawing group, significantly increasing the discharge voltage plateaus, which is 2.2 V for the parent DPDS electrode, 2.45 for 2,2′-DpyDS, and 4,4′-DpyDS, 2.8 V for DpyDSDO. The 2,2′-DpyDS with ortho-N in the pyridyl ring shows the best battery performance: 500 cycles, over 99.6% CE,

and 69% capacity retention rate. The formation of the N-Li-S coordinated bond reduces the dissolution of the discharged product of 2,2′-DpyDS in the electrolyte. (iii) Small MW PEMs with di−/tri-meric oligomers also have been reported to reduce the PEMs' solutions and increase structural stability [117]. To overcome the poor cycle retention of BQ, the dimeric BQ derivatives were used to synthesize the 2,2′-bis-p-benzoquinone (BBQ). BBQ-based cells afforded better battery performance than the polymers based on BQ such as obtaining a high specific capacity of 358 Ah kg^{-1} at first cycle and 198 Ah kg^{-1} at 50 cycles. (iv) Polymerization of small MW PEMs is a promising method to significantly stabilize the structure and extend cycling life [118]. As pointed out above, the BQ small molecule is suitable for polymeric block building because of its theoretically high working voltage of around 2.7 V and high specific capacity of 496 mAh g^{-1} based on a four-electron reaction. However, the cycling stability of BQ molecules still needs further improvement. In the experiment, the BBQ is obtained after the polymerization of BQ monomer. At the battery testing, the BQ presented a discharge voltage of 2.8 V, and first capacity of 157 Ah kg$^{-1,}$ and 20th capacity of 59 Ah kg^{-1}. In comparison, the BBQ polymer delivered a voltage of 2.9 Vm a first capacity of 326 Ah kg^{-1} and 20th capacity of 170 Ah kg^{-1}.

1.4 Morphological Engineering of PEMs

Like other materials, PEMs can also be divided into four types, including zero-dimensional (0D), one-dimensional (1D), two-dimensional (2D), three-dimensional (3D) structures [119, 120]. Morphological engineering endows PEMs with different morphologies, which highly influence their battery performances including specific capacity and power density [121–123]. Several strategies to improve the battery performances on the basis of morphological engineering are summarized in Figure 1.9.
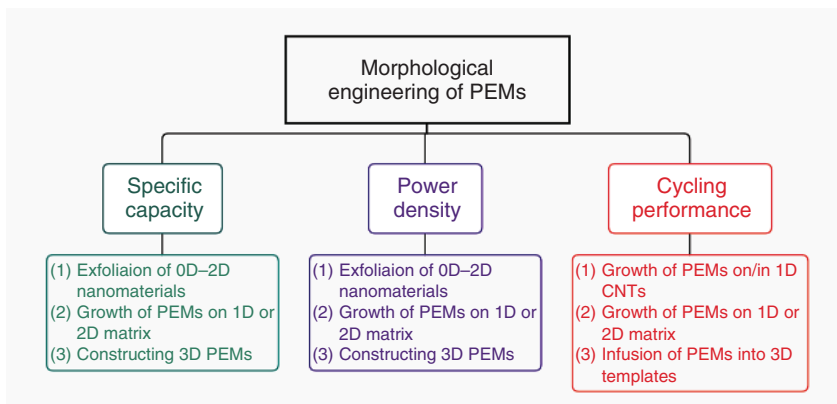

Figure 1.9 The morphological engineering strategies for PEMs to improve battery performance, such as specific capacity, power density, and cycling performance.

Based on the different PEMs fabrication methods used, the synthesis approaches of PEMs can be divided into bottom-up and top-down methods. Bottom-up fabrication is a strategy to *in situ* synthesize PEMs with various morphologies (e.g. 0D, 1D, 2D, or 3D) by stacking atoms/molecules in an ordered manner [124]. PEMs fabricated by the bottom-up method possess uniform physical structure and chemical composition, which is regarded as the ideal method to synthesize PEMs [124]. In contrast, the top-down approach is a strategy to fabricate PEMs with various morphologies through diminishing PEMs with bulky morphologies into nanoscale dimensions, which is an effective and facile method to fabricate PEMs for the convenience of obtaining bulky PEMs [124]. In the following subsections, strategies to fabricate PEMs with different morphologies through bottom-up and top-down methods are presented.

1.4.1 0D PEMs

0D PEMs can be divided into PEMs with morphologies of nanoscale particles or spherical [119]. 0D PEMs usually possess high surface area and fast ion diffusion and electron conduction kinetics, leading to high reversible capacity of batteries based on PEMs [121, 125]. Therefore, it is meaningful to summarize methods to fabricate 0D PEMs.

0D PEMs are easy to dissolve in conventional liquid electrolytes due to their large surface area and intimate contact with liquid electrolytes [119]. Therefore, increasing the molecular weight of 0D PEMs is a promising method to suppress unwanted dissolution in electrolytes, which could be achieved through *in situ* polymerization of molecular precursors [126, 127]. The shape and morphology of 0D PEMs can be controlled by changing the polarity of solvents and reaction monomers, which widens the categories of PEMs [121]. In addition, emulsion polymerization is a nascent but effective strategy to fabricate 0D PEMs with cross-linked networks for their high surface area, in which the precursor and initiator are contained in two insoluble solvents [128]. For example, 0D HCPs with diameters around 181 nm and a high surface area of $213\,m^2\,g^{-1}$ (Figure 1.10a) and LIB based on the synthesized HCP possessed a high specific capacity of $222\,mAh\,g^{-1}$ after 1000 cycles at $2\,A\,g^{-1}$ due to the high surface area and good dissolution resistance of HCP (Figure 1.10b) [128].

Nevertheless, being similar to 0D nanomaterials, most 0D PEMs are easy to aggregate into larger interconnected particles, leading to reduction of active sites of 0D PEMs and unsatisfactory loss of reversible capacity [129, 130]. Therefore, developing effective and facile bottom-up methods to fabricate 0D PEMs with good mono-dispersity is of high importance, which could be achieved through destroying the intermolecular interactions of PEMs such as hydrogen bonds and π–π interactions [131].

In addition, top-down synthesis is not only a straightforward method to obtain 0D PEMs, but also an effective way to solve the stacking problems of PEMs. The first top-down method to fabricate 0D PEMs is ball milling, which utilizes mechanical force to downsize the particle size of PEMs without damaging their chemical
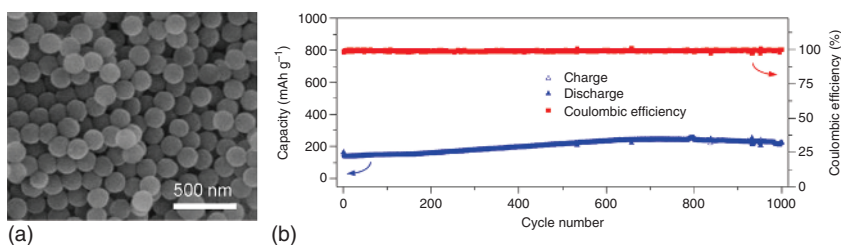
Figure 1.10 (a) SEM image of HPS. (b) Long-term cycling performance of LIB based on HPS at a current density of $2\,A\,g^{-1}$. Source: Li et al. [128], Reproduced with permission from Elsevier.

structure and composition [132, 133]. Another top-down procedure to synthesize 0D PEMs is the antisolvent method, in which bulky PEMs are first dissolved in solvent, and the solution is then dripped into another reagent to precipitate 0D PEMs [134]. Therefore, the antisolvent method is a promising method to synthesize 0D PEMs with controlled size and shape for the convenience of the procedure and the abundant versatility of bulky PEMs [36, 91].

1.4.2 1D PEMs

1D PEMs are composed of PEMs with morphologies of nanorods, nanotubes, nanowires, and nanofibers, which usually possess a high aspect ratio of length and width [119]. 1D PEMs have many advantages, such as high surface area and fast electron conduction kinetics in an ordered direction, improving the power density of batteries [119, 135]. Furthermore, growing on or diffusing into 1D CNTs could mitigate the solubility of PEMs in liquid electrolytes, endowing batteries with good long-term stability [136].

Bottom-up methods to fabricate 1D PEMs include controlled crystallization [58, 137], controlled polycondensation [138, 139], and *in situ* growth on CNT [30, 140]. The most common bottom-up synthesis method of 1D PEMs is controlled crystallization, a method where 1D PEMs are formed through self-assembly (resulting from intermolecular forces like hydrogen and π–π interactions) during the process of solvents removal [58, 137]. The morphology of 1D PEMs can also be well controlled by *in situ* polycondensation. For example, although two polyimides (PI) synthesized by *in situ* polycondensation in two different solvents exhibited 1D nanorod morphology, their diameter of nanorod was different, where PI synthesized in NMP solvent possessed a smaller diameter of 100 nm (Figure 1.11a) [139]. SIBs based on PI synthesized in NMP solvent displayed good power density and long-term cycling performances (Figure 1.11b) [139]. Another bottom-up approach for obtaining 1D PEMs is *in situ* growth on CNT [30, 140]. For instance, although COFs have a specific 2D open channel for metal ions, severe aggregation and stacking of COFs will occur due to the strong π–π interactions between COFs molecules, leading to high reduction of electroactive sites [141]. Therefore, growing layers of COFs on CNT through π–π interactions between COFs and CNT could highly hinder the self-aggregation and stacking of COFs, increasing the content of exposed active sites [141].
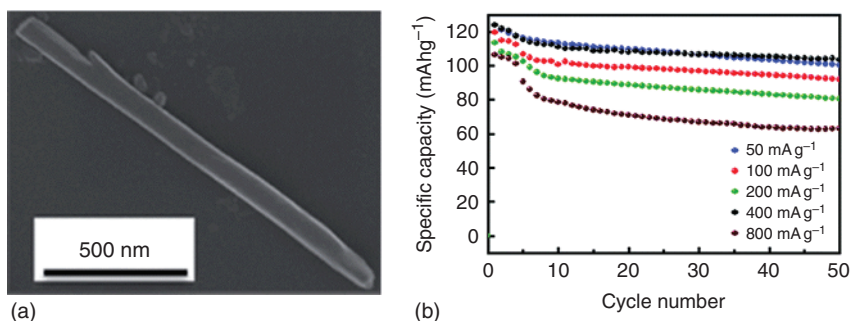
Figure 1.11 (a) HRSEM image of PI. (b) Charge–discharge cycling performance NIB based on PI at different current densities. Source: Reproduced with permission from Banda et al. [139].

In addition, top-down synthesis of 1D PEMs is composed of *ex situ* integration with CNT [136, 142, 143] and the antisolvent method [122, 144]. Most PEMs with small molecular weight exhibit high solubility in liquid electrolytes and poor electronic conductivity [145, 146]. *Ex situ* growth of 1D PEMs on CNT surfaces can be achieved through mixing and super-sonication of the mixture of PEMs and CNT in solvents. Thin layers of PEMs will subsequently form on the surface of CNT, leading to high electronic conductivity of the electrode [136]. Besides growing on the outer surface of CNTs, electro-active organic/polymers can also be injected into the inner tubular space of CNTs, diminishing the dissolution problem and improving electronic conductivity [143]. Furthermore, the antisolvent method can also be utilized to fabricate 1D PEMs with high performances, which usually display nanowire morphologies resulting from the self-assembly of molecules in one specific direction [122].

1.4.3 2D PEMs

2D PEMs are PEMs with nanosheet and nanoplate morphologies [119, 147]. 2D PEMs are promising competitors for developing high-performance batteries with their ultrahigh surface area and ultrafast in-plane electron and ion transport kinetics, endowing batteries with excellent power density and specific capacity [120, 148–150]. However, most 2D PEMs undergo severe aggregation and restacking problems, which highly decrease the content of exposed active sites, leading to reduction in power density and specific capacity of batteries [135, 151, 152]. Therefore, summarizing efficient and facile methods to synthesize 2D PEMs with high power and energy density is of great importance.

Bottom-up methods of 2D PEMs are composed of *in situ* synthesis of COFs [63, 149, 153–156], *in situ* growth on 2D matrix [157], and controlled crystallization [41, 158]. Among these three approaches, the direct bottom-up synthesis method for 2D PEMs is *in situ* synthesis of COFs [153]. As one of the most promising 2D PEMs in batteries, COFs usually exhibit fast ion diffusion rates and good long-term cycling stability for their large surface areas and stable structural skeleton [24, 149, 154]. In addition, *in situ* growth of COFs on 2D matrix, such as graphene, could strongly hinder the severe aggregation of COFs, which was achieved through replacing strong interactions between COFs layers with interactions between COFs and CNT [159].

It is worth noting that the addition of 2D matrix could decrease the energy density of batteries. Therefore, a promising method to prepare 2D PEMs is endowing PEMs with self-exfoliation ability, which could hinder self-stacking through specific inter-/intra-molecular repulsion forces [155, 160–163]. Furthermore, controlled crystallization also could be utilized to fabricate 2D PEMs, depending on both the strong intramolecular covalent force and low intermolecular van der Waals force [41].

As discussed earlier, the addition of electro-inactive components through bottom-up methods reduces the overall energy density of batteries. Fortunately, top-down synthesis could be employed to fabricate batteries with high loading of 2D PEMs [123]. The most reported top-down methods of 2D PEMs are ball milling, chemical exfoliation, super-sonication, and antisolvent methods [151, 164, 165]. Among these methods, ball milling is a frequently reported exfoliation method, which utilizes mechanical force to destroy π–π interactions between molecules of PEMs, which not only do not destruct their chemical structures and compositions, but also bestow 2D PEMs with excellent electronic conductivity and high specific capacity [166]. Chemical stripping is another top-down method to exfoliate bulky PEMs into 2D nanomaterials, which utilizes the reaction between functional moieties on PEMs and extra substance to hinder the aggregation of PEMs [167]. However, this chemical stripping method was not suitable for PEMs without reactive moieties. Super-sonication is another effective and facile method to fabricate 2D PEMs, which treats PEMs with super-sonication in high-polarity solvent, producing good 2D nanosheet morphology and endowing batteries with better power density and cycling performance [168]. Furthermore, 2D PEMs could also be fabricated through the antisolvent approach, which drips the solution containing PEMs into another solvent, and 2D PEMs with nanosheets morphology precipitate (Figure 1.12a) [62]. Batteries with 2D PEMs with nanosheets displayed ultra-stable long-term cycling performance at current density of $1.2\,A\,g^{-1}$ (Figure 1.12b), demonstrating the effectiveness of fabricating PEMs with 2D nanosheet morphology to achieve excellent battery performance [62].

1.4.4 3D PEMs

Compared with traditional inorganic active materials, most PEMs (including conductive polymers) have relatively poor electronic conductivity, leading to insufficient power density, which is a major challenge for fabricating batteries with
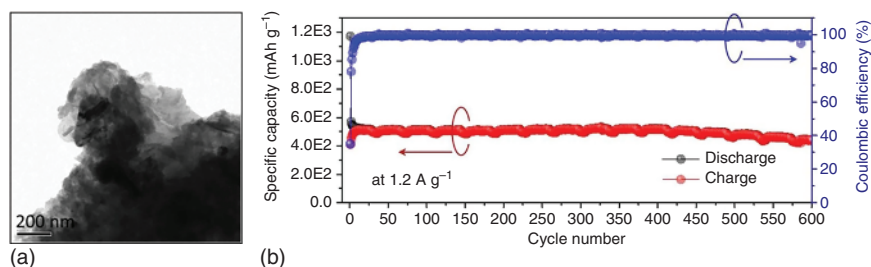

Figure 1.12 (a) TEM image of 2D PEMs with nanosheet morphology. (b) Long-term cycling performance of LIBs based on 2D PEMs. Source: Lin et al. [62], Reproduced from Elsevier.

high power density [169]. Fortunately, constructing PEMs with 3D nanostructures could not only mitigate the dissolution problem in liquid electrolytes but also improve their electronic conductivity. Many conductive matrices have been utilized to construct 3D PEMs such as CNTs, graphene, graphene oxide (GO), and reduced graphene oxide (rGO) [170–172]. As with 0-2D PEMs, 3D PEMs also could be fabricated through bottom-up and top-down methods. The conductive matrix plays a role in constructing 3D conductive networks in these processes, facilitating the enhancement of power density and capacity of batteries [82, 125].

For the bottom-up process, the precursors of PEMs mix uniformly with conductive matrix, constructing 3D PEMs, which possess intimate contact with the conductive matrix after *in situ* polymerization [89, 173–175]. Therefore, 3D PEMs usually display high electronic conductivity and low resistance. Nevertheless, the excessive introduction of conductive matrix highly decreases the energy density of batteries, hindering their large-scale practical application [176]. Therefore, fabricating 3D PEMs with excellent battery performance but with little addition of conductive templates is a difficult task to accomplish.

Apart from bottom-up methods, top-down approaches also could be utilized to synthesize 3D PEMs by dispersing bulky PEMs on templates. This process could not only mitigate the dissolution of some PEMs (especially PEMs with low molecular weight) in electrolytes, but also make it possible to construct flexible and free-standing 3D PEMs [177–179]. Moreover, ideal PEMs of batteries should not contain any extra inactive substances, such as binder and current collector, which could greatly decrease the weight of batteries and increase their overall energy densities. Among conductive matrices, CNT and GO derivatives are good templates to fabricate flexible and free-standing 3D PEMs, which not only do not need extra addition of electro-inactive binder and metal current collector, but also guarantee high electronic conductivity of 3D PEMs and excellent power density and high capacity/energy densities of batteries [180]. For example, a 3D flexible and free-standing PEM was synthesized by filtrating the mixture of PEMs and CNTs (Figure 1.13a), which did not introduce any binder, exhibiting ultrahigh specific capacity and power density (Figure 1.13b), demonstrating the promising potential of 3D PEMs for fabricating future high-performance batteries [181].
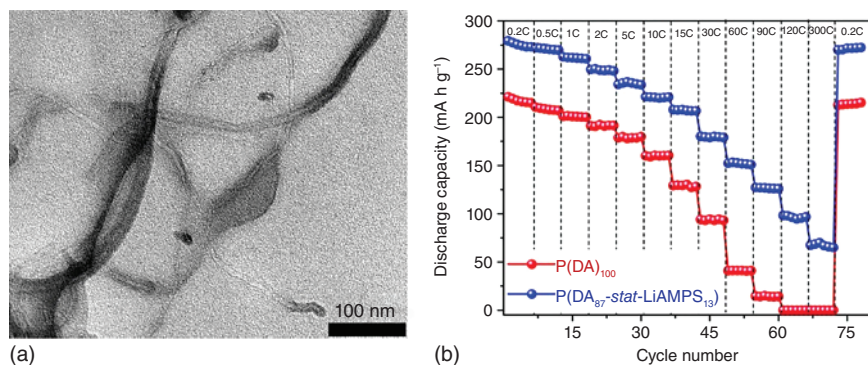

Figure 1.13 (a) TEM image of 3D flexible and freestanding PEMs. (b) Power densities of LIBs based on 3D flexible and freestanding PEMs. Source: Patil et al. [181], Reproduced with permission from John Wiley & Sons.

1.5 Applications of PEMs

1.5.1 LIBs

Hitherto, LIBs were the most promising rechargeable batteries for their high energy/power densities and long cycle life [16, 17, 182, 183]. LIBs have been applied to many modern commercial products such as green electric vehicles and portable electronics [184–186]. To obtain high energy densities, LIBs could employ lithium metal as the anode for its high specific capacity ($\approx$3860 mAh g^{-1}) and low redox potential of Li/Li$^+$ (-3.04 V) versus standard hydrogen electrode (SHE) [13, 187–189]. Compared with traditional inorganic electrode materials, PEMs are considered promising candidates for fabricating future high-performance LIBs due to their low cost, structural diversity, tunable properties, and environmental benignity. Even though PEMs have some drawbacks, many representatives of PEMs have demonstrated the great potential of PEMs for constructing advanced LIBs with high power and energy density.

COFs have been considered one of the most promising PEMs candidates for their 2D open channels and stable polymeric frameworks. Wang et al. synthesized an anthraquinone-based COF called DAAQ-TFP-COF, which possessed high content of carbonyl active sites [166]. However, the synthesized DAAQ-TFP-COF exhibited bulky and opaque morphology, indicating carbonyls active sites of DAAQ-TFP-COF were buried among COF layers due to the strong intermolecular π–π interactions [166]. After ball milling, DAAQ-TFP-COF was delaminated into DAAQ-ECOF with 2D few-layer nanosheets, which exhibited high surface area of 216 m^2 g^{-1} [166]. LIBs based on DAAQ-ECOF displayed much better power density and long-term cycling performance compared to that based on DAAQ-TFP-COF, demonstrating the higher content of carbonyl active sites of DAAQ-ECOF after ball milling [166]. Nevertheless, the electronic conductivities of conventional COFs are much lower than those of inorganic electrode nanomaterials.

Compositing with 1D conductive nanomaterials, such as CNTs, through bottom-up methods is an effective way to increase the electronic conductivity of PEMs. Cooper et al. synthesized a COF named DAPQ-COF, which had adjacent carbonyl groups [190]. Two types of composite COFs were fabricated through *in situ* and *ex situ* mixing with CNT [190]. The first composite COF was DAPQ-COF/CNT, which was fabricated through simply mixing DAPQ-COF with CNT by ball milling, and the interface between DAPQ-COF and CNT was not intimate [190]. The second composite COF was DAPQ-COFX (X indicated the content of CNT in the mixture of CNT and DAPQ-COF), which was prepared through *in situ* polymerization of DAPQ-COF precursors with CNT (Figure 1.14a) [190]. DAPQ-COF50 exhibited core–shell 1D morphology with the core of CNT and the shell of DAPQ-COF, in which the DAPQ-COF was grown closely on the outer side of CNT [190]. LIB based on DAPQ-COF50 displayed stable long-term cycling performance with capacity retention of 76% after 3000 cycles at 2 A g^{-1}, indicating the stable composite structure of DAPQ-COF50 [190]. In comparison with LIB based on DAPQ-COF/CNT, LIB with DAPQ-COF50 exhibited higher utilization of active sites (95%) and much
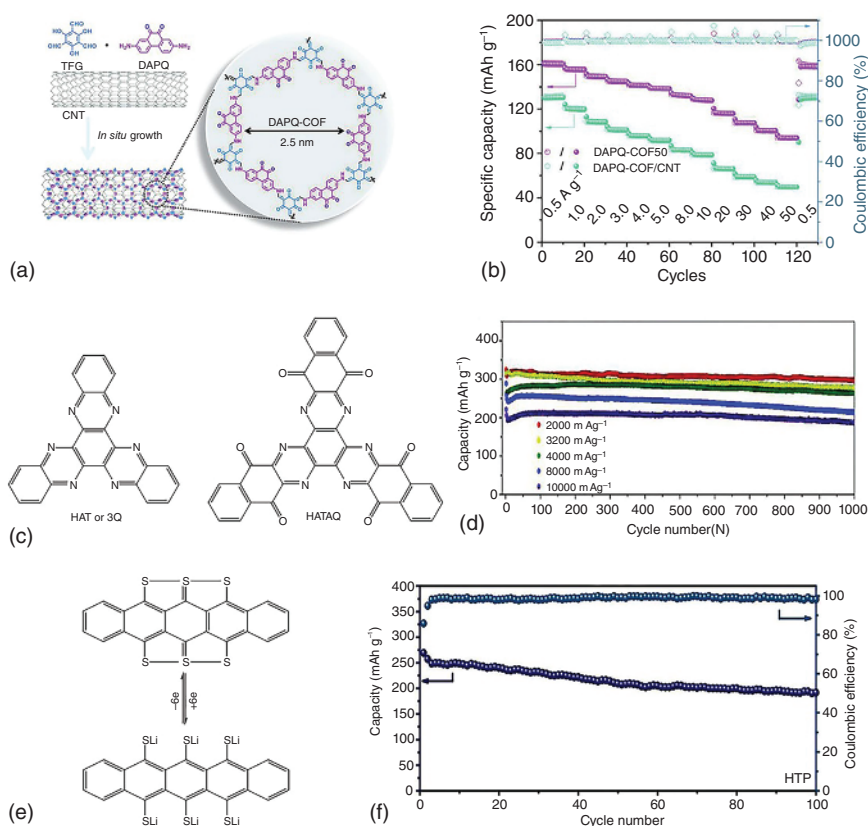
Figure 1.14 (a) Schematic illustration of fabrication route of DAPQ-COF50. (b) Power density of LIBs based on DAPQ-COF50 and DAPQ-COF/CNT. Source: Gao et al. [190]/Public Domain/CC BY 4.0. (c) Chemical structure of HATAQ. (d) LIB based on HATAQ at various current densities. Source: Reproduced from Ref. [191]. Copyright 2021, WILEY-VCH Verlag GmbH & Co. KGaA, Weinheim. (e) Charge storage mechanism of HTP. (f) Power density of LIB based on HTP. Source: Reproduced from Ref. [192]. Copyright 2019, WILEY-VCH Verlag GmbH & Co. KGaA, Weinheim.

better power density (94 mAh g^{-1} at 50 A g^{-1}), demonstrating the advantages of bottom-up methods over top-down methods for fabricating high-performance batteries with composite PEMs (Figure 1.14b) [190].

Imine-containing PEMs are another candidate for constructing high-performance LIBs. 5,6,11,12,17,18-hexaazatrinaphthyl-ene (HAT) had multiple active sites, and LIBs based on HAT exhibited good power density and stable long-term cycling performance for the electron-deficient core structure and π-extended framework [58]. In order to further extend the conjugation system and increase the content of redox active sites, Kaveevivitchai et al. synthesized a HAT quinone called HATAQ by introducing benzene ring and quinone moiety into the structure of HAT (Figure 1.14c) [191]. LIB based on HATAQ displayed excellent long-term cycling performance with a high specific capacity of 209 mAh g^{-1} and capacity retention of

84.6% after 1000 cycles at $10\,A\,g^{-1}$ (Figure 1.14d), which may result from the fast charge transfer kinetics derived from the extended π-conjugated structure [191]. Nevertheless, the mass loading of active material in HATAQ electrode was only 30%, which was far from the requirement of practical battery application. Therefore, fabricating PEMs with the core structure of HATAQ may have not only better electronic conductivity but also fewer dissolution problems in liquid electrolytes due to their polymer skeleton. To reduce dissolution and increase the utilization of active sites of PEMs, Feng et al. synthesized a composite 2D carbon-linked nanoporous conjugated polymer framework named hexaazatrinaphthalene (CCP-HATN)@CNT through *in situ* polymerization of precursors of CCP-HATN with CNT, which highly prevented the self-stacking of HATN and increased the electronic conductivity of HATN [193]. LIB with CCP-HATN/CNT cathode displayed high utilization of active sites (73%) due to the excellent electronic conductivity of CNT [193]. LIBs based on CCP-HATN/CNT cathode exhibited stable long-term cycling performance with capacity retention of 91% after 1000 cycles at $0.5\,A\,g^{-1}$, demonstrating the good dissolution resistance of CCP-HATN/CNT in electrolyte due to its 2D robust nanoporous polymer structure [193].

Sulfur-containing PEMs could also be utilized as advanced electrodes to fabricate high-performance LIBs with the mechanism of reversible breakage and regeneration of S–S bond. However, most sulfur-containing substances utilized in batteries have low molecular weight and usually suffer from severe dissolution problems. Long et al. synthesized a trisulfide hexathiapentacene (HTP) through mixing, well-grounding, and subsequently high-temperature annealing in a facility based on zone-melting chemical vapor transport (ZM-CVT) [192]. Then, HTP single crystal was obtained through evaporation and condensation processes, which exhibited special 1D morphology (Figure 1.14e) [192]. LIBs based on HTP displayed good power density, which retained a specific capacity of $181\,mAh\,g^{-1}$ at 1 C (Figure 1.14f), demonstrating the fast charge transfer kinetics within the HTP electrode [192]. LIBs based on HTP exhibited relatively stable long-term cycling performance, which possessed capacity retention of 72% after 100 cycles at 0,1 C, indicating that the breakage and regeneration of S-S bonds in HTP were reversible during continuous charge–discharge processes [192]. Nevertheless, the long-term cycling performance of batteries based on HTP molecules was far from practical application, indicating that fabricating PEMs based on a precursor of HTP was a meaningful and practical method to hinder the parasitic dissolution of HTP.

Radical PEMs are another electrode for preparing LIBs with high power densities due to their slight variation of structure and electron rearrangement during the electrochemical process. Blinco et al. synthesized a radical PEM named poly(5-vinyl-1,1,3,3-tetramethylisoindolin-2-yloxyl) (PVTMIO) through three-step chemical reactions, which could achieve reversible transition between oxoammonium cation and nitroxyl moiety during the charge and discharge process [194]. LIBs based on PVTMIO exhibited excellent power density, which could retain 55% of the specific capacity ($68.4\,mAh\,g^{-1}$) at 100 C in comparison with that at 1 C due to the fast charge transfer kinetics and low polarization within the PVTMIO electrode [194]. However, the mass loading of PVTMIO within the electrode was only

10%, and a large quantity of conductive carbon (40%) was added into the electrode due to the insulating feature of PVTMIO, which is far from the requirements of practical battery application [194]. Therefore, future radical PEMs should improve their electronic conductivity, such as grafting nitroxyl side chains, onto the main chain of conductive polymers.

Conducting polymer PEMs, such as poly (thiophene) (PT), have attracted much attention for their high electronic conductivities and reversible redox behavior. Nevertheless, some conducting polymer PEMs exhibited low redox activity and poor power density due to the relative instability of conducting polymer PEMs. Jiang et al. synthesized a conjugated microporous polymer (CMP) called poly(3,3′-bithiophene) (P33DT), which possessed high density of thiophene [195]. In comparison with PT with linear polymer structure and low surface area ($13\,m^2\,g^{-1}$), P33DT possessed cross-linked polymer network and high surface area ($168\,m^2\,g^{-1}$) due to the less stacking among polymer chains in P33DT [195]. In addition, LIBs based on P33D displayed excellent power density ($387\,mAh\,g^{-1}$ at $5\,A\,g^{-1}$) and retained specific capacity of $663\,mAh\,g^{-1}$ after 1000 cycles at $500\,mA\,g^{-1}$, demonstrating the effectiveness of increasing surface area for improving battery performance [195].

1.5.2 SIBs

Even though LIBs exhibited high power and energy density, society could not sustain further consumption of lithium reserves due to the uneven distribution and high cost of lithium reserves, indicating the necessity for fabricating novel energy storage systems [196–200]. Among these novel renewable energy systems, SIBs have attracted extensive attention and are considered as one of the most promising alternatives to LIBs due to the similar chemical properties between sodium and lithium elements [201]. In addition, sodium is abundant in the Earth's crust and is distributed uniformly, which endows SIBs with low cost compared with LIBs and promotes the large-scale application of SIBs. Compared with LIBs, SIBs usually display relative low power density due to the large radius of Na^+. Fortunately, many PEMs could achieve fast and reversible electrochemical processes for their flexible structures and low variation of volume during charge/discharge process.

Radical intermediates will generate during sodiation/desodiation process, which are unstable and easy to transform into inactive compounds by reacting with other molecules in the electrolyte, leading to poor battery performance [202]. Lu et al. stabilized the transition between —C=O and —C—O—Na of tri-b-ketoamine through forming —NH— moiety by reacting with another compound [202]. As the neighboring group of —C=O, —NH— had a resonance effect on the radical intermediate, which could prevent radical intermediates from reacting with other molecules in electrolyte [202]. The rigid structure of synthesized molecules also has a strong steric hindrance effect on severe irreversible intermolecular reactions between radical intermediates, leading to improvement of stability of radical intermediates [202]. Therefore, SIBs based on the synthesized tris(N salicylideneanthraquinoylamine) (TSAQ) displayed a high specific capacity over $250\,mAh\,g^{-1}$ after 2000 cycles at
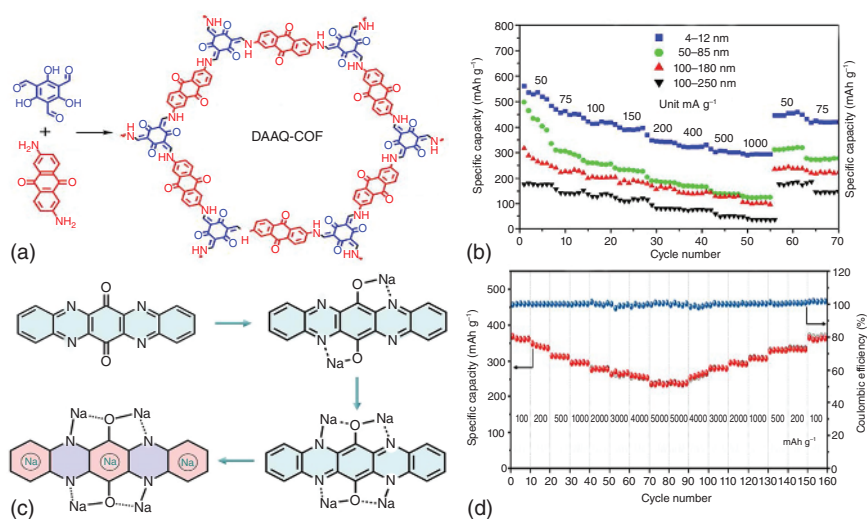
Figure 1.15 (a) Synthetic route of DAAQ-COF. (b) Power densities of SIBs based on DAAQ-COF with various thicknesses. Source: Reproduced from Ref. [151]. Copyright 2019, American Chemical Society. (c) Proposing storage mechanism of TAPQ. (d) Power density of SIB based on TAPQ anode with diglyme-based electrolyte. Source: Reproduced from Ref. [203]. Copyright 2021, WILEY-VCH Verlag GmbH & Co. KGaA, Weinheim.

a high current density of $1000 \, \text{mA g}^{-1}$, demonstrating the ultra-stable chemical structure of TSAQ radical intermediates and reversible transition between —C=O and —C—O—Na during long-term cycling processes [202]. In order to further increase the specific capacity of PEMs, Lu et al. prepared a COF named DAAQ-COF through polycondensation (Figure 1.15a), which provided 2D open channel for Na$^+$ diffusion [151]. Different top-down methods, such as ball milling and antisolvent, were used to delaminate DAAQ-COF into few-layer stacking 2D COF due to the strong van der Waals forces and π–π interactions among DAAQ-COF layers [151]. Among these DAAQ-COF samples after top-down treatment, DAAQ-COF with thickness between 4 and 12 nm was prepared by antisolvent method with methane-sulfonic acid as solvent and methanol as antisolvent [151]. SIBs based on DAAQ-COF with thickness of 4–12 nm performed better than those based on DAAQ-COF with denser thickness (Figure 1.15b), because dense DAAQ-COF layers buried some active sites of DAAQ-COF and hindered the Na$^+$ diffusion [151]. SIBs based on DAAQ-COF with thickness of 4–12 nm exhibited ultra-stable long-term cycling performance with high capacity retention of 99% after 10 000 cycles at $5 \, \text{A g}^{-1}$ owing to the resonance effect of —NH— moiety and stable COF structure, indicating an inspiring way to fabricate PEMs with high power and reversible capacity [151].

Imine-containing PEMs are good candidates as anode of SIBs due to their low reaction potentials. However, imine-containing organic materials, especially for those with small molecular weight, usually exhibit poor battery performance due to parasitic dissolution in conventional electrolytes. The first strategy to mitigate

the dissolution of imine-containing organic materials in electrolyte is fabricating organic sodium salts. For example, Wang et al. synthesized an azo compound called azobenzene-4,4′-dicarboxylic acid sodium salt (ADASS), which exhibited low solubility in electrolyte due to the existence of carboxylate group in azobenzene [204]. SIBs based on ADASS displayed good power density with specific capacity of 71 mAh g^{-1} at 20 C, which may result from the extended conjugated structure [204]. SIBs with ADASS anode exhibited ultra-stable long-term cycling performance with specific capacity of 98 mAh g^{-1} after 2000 cycles at 20 C, demonstrating the ultralow solubility of ADASS in electrolyte and stable chemical structure during charge/discharge processes [204].

The second way to mitigate the solubility of imine-containing organic materials in electrolyte is regulating electrolyte composition. For instance, Zhang et al. synthesized a N-heteropentacenequinone (TAPQ), which had not only imine moiety but also carbonyl groups on its chemical structure, and multiple Na$^+$ storage was expected according to the anticipated mechanism (Figure 1.15c) [203]. SIBs based on TAPQ anode with carbonate-based electrolyte exhibited fast capacity fading due to the structure damage of TAPQ in carbonate-based electrolyte [203]. On the other hand, SIBs based on TAPQ anode with diglyme-based electrolyte displayed high capacity of 72% after 1000 cycles at 1 A g^{-1}, indicating the good structural stability of TAPQ in dielyme-based electrolyte [203]. SIBs with TAPQ anode in diglyme-based electrolyte possessed much better rate capacity than that in carbonate-based electrolyte (Figure 1.15d), confirming the great influence of electrolyte composition on structural stability of PEMs and battery performances [203]. However, these imine-containing organic materials with small molecular weight still exhibit parasitic dissolution in some liquid electrolytes, confirming the necessity of fabricating imine-containing PEMs which could combine advantages of excellent stability and high specific capacity.

Several PEMs have unsatisfactory battery performance, such as low power density, due to the large radius of Na$^+$ and insulation feature of PEMs. However, radical PEMs, such as poly(2,2,6,6-tetramethylpiperidinyloxy-4-vinylmethacrylate) (PTMA), could achieve high power density in SIBs, because of the fast transition rate between their oxidized (oxoammonium cation) and reduced (trioxide radical) state, which has little volume change during charge/discharge processes. But most radical PEMs suffer from severe fast self-discharge problems due to their parasitic dissolution in electrolyte [143]. Kim et al. fabricated a PTMA-CNT composite PEM through diffusing PTMA into the inner space of CNT [143]. CNT played two important roles in PTMA-CNT composite PEM: firstly, CNT could form an intimate interface with PTMA due to the π–π interaction between CNT and PTMA, leading to enhancement of charge transfer kinetics [143]. CNT could also mitigate the dissolubility of PTMA in electrolyte for the π–π interaction between them, resulting in stable long-term cycling performance [143]. Therefore, SIBs based on PTMA showed high power density, with a specific capacity of 190 mAh g^{-1} at 5 C and high capacity retention of 92% after 100 cycles in long-term cycling characterization investigated at 0.5 C, demonstrating the benefits of 1D CNT for enhancement of battery power density [143].

1.5.3 PIBs

Many reported inorganic electrode materials, such as intercalation-type, conversion-type, and alloy-type materials, suffer from large volume change during electro-chemical processes due to the large radius of K$^+$, leading to parasitic structural collapse of inorganic electrode materials and fast loss of capacity. PEMs enjoy many advantages over inorganic electrode materials such as various structural diversity, good property designability, and low volume expansion during charge/discharge processes [41]. Nevertheless, PEMs in PIBs exhibit low power density, relatively low capacity, and long-lasting stability [41]. Fortunately, some strategies have been developed to increase the power density and long-term cycling performance such as fabricating 2D PEMs [41], polymerizing precursors [205], and forming organic salts [206].

The first strategy to enhance the battery performances of PIBs based on organic materials with carbonyl-containing moiety is constructing lamellar morphology. For example, Tang et al. synthesized a lamellar tetrapotassium pyromellitic (K$_4$PM) with four conjugated carboxylate groups by neutral reaction between pyromellitic acid and KOH (Figure 1.16a) [41]. Subsequently, raw K$_4$PM was ball-milled with conductive carbon to achieve intimate interface between K$_4$PM and conductive carbon and
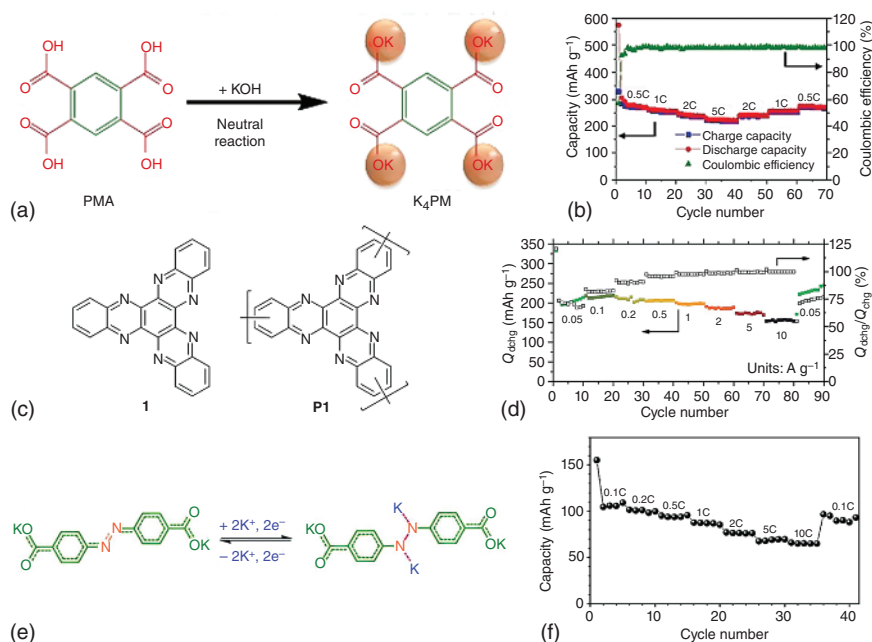
Figure 1.16 (a) Synthesis route of K$_4$PM. (b) Power density of PIB based on K$_4$PM. Source: Reproduced from Ref. [41]. Copyright 2021, WILEY-VCH Verlag GmbH & Co. KGaA, Weinheim. (c) Chemical structures of 1 and P1. (d) Power density of PIB based on P1. Source: Reproduced from Ref. [207]. Copyright 2019, The Royal Society of Chemistry. (e) K$^+$ storage mechanism during charge/discharge process in PIB. (f) Power density of PIB based on ADAPTS. Source: Reproduced from Ref. [206]. Copyright 2019, WILEY-VCH Verlag GmbH & Co. KGaA, Weinheim.

high utilization of redox-active sites on K_4PM [41]. PIBs based on K_4PM exhibited excellent power density with high specific capacity of 223 mAh g^{-1} at 5 C, which result from the lamellar morphology of K_4PM and intimate contact between K_4PM and inorganic conductive carbon (Figure 1.16b) [41]. PIBs with K_4PM anode displayed high capacity retention of 83% after 1000 cycles at 500 mA g^{-1}, and the good stability of PIB derived from the stable conjugated π systems of four carboxylate groups on K_4PM [41]. Nevertheless, its long-term cycling stability was still far from the requirements of practical applications, which could be improved by fabricating PEMs with lamellar morphology.

The second way to improve the power density and mitigate the dissolution problem of PEMs is polymerizing precursors with high molecular weight [174]. For instance, a series of polyimide PEMs with different lengths of alkyl chains were synthesized through polycondensation between 3,4,9,10-perylene-tetracarboxylic acid-dianhydride (PTCDA) and alkyl diamine [208]. PIBs with the optimized polyimide PEMs exhibited high power density with energy density of 113 Wh kg^{-1} at 147.06 C, which was the result of fast charge transfer capability derived from the extended π conjugated system of polyimide [208]. PIBs with the optimized polyimide PEMs displayed ultra-stable long-term cycling performance with no obvious capacity loss after 1000 cycles at 7.35 C, indicating high dissolution resistance and structure stability of polyimide PEMs during charge/discharge processes [208]. In addition, although both LIBs and SIBs based on triquinoxalinylene 1/GO composite PEMs displayed high power density and long-term cycling performance, the expensive cost of GO hindered the further application of triquinoxalinylene 1 in the battery system [207]. Therefore, Troshin et al. synthesized an analogue of triquinoxalinylene 1 called polymer 1 (P1) through polymerization polymer precursor (Figure 1.16c), which exhibited nanoparticle morphology with size about 200–500 nm [207]. PIBs based on P1 displayed excellent power density with a specific capacity higher than 150 mAh g^{-1} at 10 A g^{-1} (Figure 1.16d), which was derived from the extended π conjugated system and fast charge transport dynamic of P1 [207]. PIBs with P1 cathode retained high specific capacity of 169 mAh g^{-1} after 4600 cycles at 10 A g^{-1}, demonstrating the stable molecule structure of P1 during long-term electrochemical processes derived from the lower dissolution of P1 in electrolyte [207].

Another effective strategy to mitigate the dissolution of organic materials in the electrolyte of PIBs is forming organic salts [206]. For instance, Wang et al. synthesized azobenzene-4,4′-dicarboxylic acid potassium salts (ADAPTS) with lamellar morphology through the acid–base reaction between azobenzene-4,4′-dicarboxylic acid and KOH, which could highly reduce its dissolution in the polar organic electrolyte in PIB and could achieve reversible K$^+$ storage behavior (Figure 1.16e) [206]. PIBs based on ADAPTS exhibited good power density with a high specific capacity of 66 mAh g^{-1} at 10 C (Figure 1.16f), demonstrating the benefit of the lamellar morphology and reduced dissolution of ADAPTS in electrolyte for high electron transport speed [206]. Moreover, PIBs with ADAPTS anodes were investigated at high temperature (50 °C and 60 °C) and possessed better battery performances than those with ADAPTS anodes investigated at ambient temperature due to the faster

electron conduction at a higher temperature, which further demonstrated the broad application of ADAPTS in PIB systems [206]. Furthermore, the long-term cycling performance of batteries based on ADAPTS could be improved further by fabricating PEMs with the core structure of azobenzene through polymerization.

1.5.4 Multivalent MIBs

Compared with conventional LIBs, SIBs, and PIBs, rechargeable multivalent metal-ion batteries (MIBs) with aqueous electrolytes enjoy many advantages such as cost efficiency, high volumetric energy density, reserve abundance, and environmental benignity [209]. Although MIBs have many advantages, they still suffer from several challenges, one of them being the undesired cathode materials. Unlike monovalent metal ions (such as Li^+, Na^+, and K^+), the charge carriers in aqueous electrolytes are hydrated multivalent metal ions [209]. Even though both desolvated and solvated multivalent metal ions could interact with the cathode through insertion/deinsertion, it is difficult for hydrated multivalent metal ions to insert into the cathode due to the large radius of hydrated multivalent metal ions and small/rigid channels of inorganic cathode materials [209]. Therefore, these hydrated multivalent metal ions could achieve redox reactions with cathodes after desolvation. Nevertheless, the desolvation process of hydrated multivalent metal ions requires large energy consumption due to their high charge density, leading to sluggish reaction kinetics and unsatisfactory battery performances [209]. In addition, some representative inorganic cathode materials, such as transition metal oxides and transition metal phosphates, have rigid crystal structures, which could cause irreversible structural collapse after huge volume changes during continuous charge/discharge processes, resulting in poor cyclic stability [210]. Moreover, the high electrostatic interaction between multivalent metal ions and cathode hosts causes sluggish diffusion kinetics of multivalent metal ions [210]. Therefore, the selection of suitable inorganic cathode materials for MIBs is a big challenge due to the high charge density, large radius of hydrated multivalent metal ions, and huge volume change during the electrochemical process.

As discussed previously, PEMs possess many advantages for MIBs application, such as tunable and flexible chemical structure, which could facilitate the diffusion of multivalent metal ions and anions in aqueous electrolyte [210]. In addition, the redox reactions between PEMs and multivalent metal ions only cause the change of valence bond instead of huge volume change, benefiting fast reaction kinetics and good cycling stability of MIBs. In the following section, representative PEMs utilized in MIBs will be introduced and discussed in the sequence of different storage mechanisms of PEMs to clarify the "structure-performance" relationship between PEMs and MIBs. Important perspectives for the development of high-performance MIBs with advanced PEMs will also be provided.

1.5.4.1 Conducting Polymers

Compared with conventional inorganic cathode materials, conducting polymers show better electronic conductivity for their long-range π-conjugated systems,
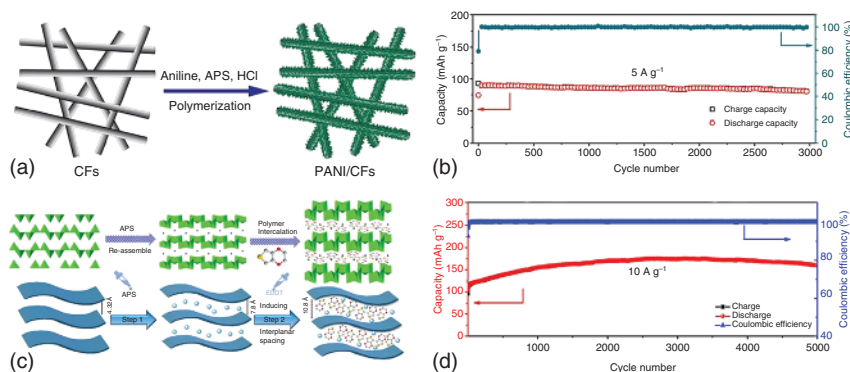
Figure 1.17 (a) Preparation route of PANI/CFs. (b) Long-term cycling performance of ZIB based on PANI/CFs. Source: Reproduced from Ref. [75]. Copyright 2018, WILEY-VCH Verlag GmbH & Co. KGaA, Weinheim. (c) Schematic illustration of the preparation of PEDOT-intercalation NVO-layered material. (d) Long-term cycling performance of ZIB based on PEDOT-NVO cathode. Source: Reproduced from Ref. [212]. Copyright 2020, Elsevier Science B.V.

which facilitate electron transport within the cathode, resulting in a high power density of rechargeable zinc ions battery (RZIBs) [211]. The most frequently reported conducting polymer is polyaniline (PANI) for its facile synthetic route, fast electron transport speed, and good flexibility. Chen et al. fabricated a freestanding and porous cathode (PANI/CFs) through *in situ* polymerization of the precursor of PANI on the surface of carbon fiber (Figure 1.17a) [75]. The PANI/CFs cathode showed a nano-thorn structure, which could facilitate the infiltration of aqueous electrolyte into the cathode, leading to low Zn^{2+} diffusion barrier [75]. RZIBs with PANI/CFs cathode exhibited excellent rate capacity at the current density from 0.05 to $5\,A\,g^{-1}$, and a high capacity of $82\,mAh\,g^{-1}$ was retained after 3000 cycles at a current density of $5\,A\,g^{-1}$ (Figure 1.17b), demonstrating its promising potential as high-performance cathode materials of RZIBs [75]. It is worth noting that the electrolyte utilized in this RZIB is $Zn(CF_3SO_3)_2$, which is much more expensive than $ZnSO_4$. Nevertheless, oxidized PANI will react with water molecules in $ZnSO_4$, resulting in fast capacity fade [75]. Therefore, it is critical to develop strategies to prepare stable PANI in traditional $ZnSO_4$ aqueous electrolytes. Another issue is that high proton concentration should be guaranteed to enable the reversible redox reaction of PANI in aqueous electrolyte [213]. A high acidic environment will corrode the Zn metal anode, leading to fast fade of battery performance [213]. Sun et al. synthesized a novel PANI material with —SO_3^- group through copolymerization between aniline and metanilic acid on carbon cloth, which could ensure a high acidic local environment in low acidic aqueous electrolyte [213]. A high capacity ($110\,mAh\,g^{-1}$) was obtained after 2000 cycles at a high current density of $10\,A\,g^{-1}$, pointing out the effectiveness of the introduction of —SO_3^- group on battery performance [213].

Even though RZIBs with PANI cathode exhibited fast power density and stable long-term cycling performance, the specific capacity of RZIBs is far from practical application. The capacity of RZIBs with traditional inorganic cathode

materials also fades quickly in high charge–discharge depth due to the serious structural collapse of inorganic cathode materials during the charge/discharge processes [214]. Therefore, fabricating composite cathode with PANI and inorganic cathode materials with high theoretical capacity is a promising way to accomplish high power density, good cycling stability, and high specific capacity. Xia et al. fabricated PANI-intercalated MnO_2 nanolayers through facile interface reactions, in which PANI could strengthen the extended layered structure of MnO_2 and facilitate electron transport due to the excellent electronic conductivity of PANI [214]. Benefiting from the combined advantages of both PANI and MnO_2, RZIBs with PANI-intercalated MnO_2 cathode exhibited high capacity (280 mAh g^{-1}) after 200 cycles at 200 mA g^{-1}, which was the highest utilization of MnO_2 based on all the reported literature [214]. Xia et al. fabricated a novel poly(3,4-ethylenedioxythiophene) (PEDOT)-intercalated ammonium vanadate oxide (NVO) through *in situ* polymerization of the precursor of PEDOT with NVO (Figure 1.17c) [212]. In this novel PEDOT-intercalated NVO composite cathode, PEDOT extended the interlayer spacing of NVO from pristine 7.8 Å to 10.8 Å, which facilitated the diffusion of cations in the aqueous electrolyte into the inner sites of the crystal lattice of NVO, leading to the better utilization of active sites [212]. RZIBs with PEDOT-intercalated NVO composite cathode displayed a high capacity of 160.6 mAh g^{-1} with negligent capacity loss (94.1% of the highest capacity) after 5000 cycles at 10 A g^{-1} (Figure 1.17d). This excellent long-term cycling performance was superior to most reported RZIBs, demonstrating the vast potential of fabricating composite cathode [212].

1.5.4.2 Carbonyl Compounds

Another type of PEMs utilized in RZIBs are carbonyl compounds, and the reversible redox reactions could be achieved through fast and reversible enolization reactions (two carbonyl groups combine one Zn^{2+}), leading to a high power density of RZIBs [215]. However, some PEMs, especially those with low molecular weight, are inherently unstable and suffer from parasitic solubility in mild aqueous electrolyte, resulting in the crossover of PEMs between cathode and anode and poor battery stability [215]. Most reported works indicate that organic materials with low molecular weight will have poor battery performance due to their parasitic dissolution in mild aqueous electrolytes [216, 217]. However, Sun et al. synthesized a small molecule quinone with four amino groups named tetraamino-p-benzoquinone (TABQ), which exhibited good anti-dissolution ability due to the hydrogen bond interactions between the carbonyl group and amino group [218]. The continuous hydrogen bonding network also facilitated fast proton conduction, resulting in low activation energy for proton transfer and diffusion [218]. SEM images showed that TABQ was homogeneously coating the surface of conductive additives as a thin layer, guaranteeing good electronic conductivity within the cathode [218]. Benefiting from the novel hydrogen bonding network, symmetric chemical structure, and low molecular weight, RZIB with TABQ active materials displayed a high capacity of 213 mAh g^{-1} after 1000 cycles at 5 A g^{-1}, demonstrating the significance of the molecular structure of PEMs for the improvement of battery performance [218].

However, the capacity of batteries with TABQ is quickly lost at low current density, which may result from the dissolution of the intermediate product of TABQ during the charge/discharge processes [218]. Therefore, fabricating PEMs with the precursor of TABQ could stabilize the chemical/electrochemical stability of organic materials during the continuous electrochemical process.

Developing PEMs or compounds with higher molecular weight is another way to solve the parasitic dissolution problem of most PEMs in the aqueous electrolyte of MIBs. For example, Choi et al. synthesized a tetradiketone (TDK) macrocycle with three pairs of adjacent carbonyl groups, and each pair of adjacent carbonyl groups could form a chelate with one $AlCl^{2+}$ [219]. Although TDK could still be dissolved in electrolyte, the acetylene carbon could highly hinder its dissolution [219]. AIBs based on TDK cathode displayed good power density with a high specific capacity of $66\,mAh\,g^{-1}$ at $2\,A\,g^{-1}$, demonstrating its fast electron/ion diffusion kinetics [219]. AIBs with TDK cathode also retained a high capacity retention of 78% after 8000 cycles at $1\,A\,g^{-1}$, which further confirmed the long-term chemical/electrochemical stability of TDK during the electrochemical process in AIBs [219]. In addition, Stoddart et al. synthesized a novel redox-active triangular phenanthrenequinone-based macrocycle (PQ-Δ), which was insoluble in common solvents and could achieve reversible redox reactions between adjacent carbonyl groups with $AlCl_2^+$ [220]. AIBs based on PQ-Δ exhibited excellent power density with a high specific capacity of $70\,mAh\,g^{-1}$ at $10\,C$, which may result from the well-defined channel formed by the π–π interactions among PQ-Δ [220]. AIBs with PQ-Δ cathode also displayed ultra-stable long-term cycling performance with a high specific capacity of $53\,mAh\,g^{-1}$ after 5000 cycles at $20\,C$, which further demonstrated the great potential of PQ-Δ for high-performance and affordable AIB systems [220]. All these works indicate the promising potential of carbonyl PEMs for fabricating high-performance MIBs.

Furthermore, polymer-based PEMs were prepared and utilized as cathode materials of RZIBs to confront their dissolution issue [221]. Alshareef et al. developed a strategy to enhance the electrochemical performance of RZIBs by introducing the quinone group into the chemical structure of the covalent organic framework (HAQ-COF), which had a relatively high surface area of $53\,m^2\,g^{-1}$ [222]. Owing to the 2D open channels of HAQ-COF, ZIBs based on HAQ-COF exhibited excellent power density with a high specific capacity of $95.6\,mAh\,g^{-1}$ at $10\,A\,g^{-1}$ [222]. ZIBs with HAQ-COF cathode retained a high specific capacity of $128\,mAh\,g^{-1}$ after $10\,000$ cycles at $5\,A\,g^{-1}$, demonstrating the stable chemical structure and reversible redox reaction of HAQ-COF in ZIBs [222]. Moreover, it was evident that molecular engineering plays an important role in increasing the practical charge storage performance of ZIBs.

1.5.4.3 Imine Compounds

As one of the PEMs in RZIBs, imine compounds could also achieve high cation storage by combining with Zn^{2+} through C=N group during discharge processes [223, 224]. Previous research revealed that organic materials with small π-conjugated systems will restrict the electrochemical performance of
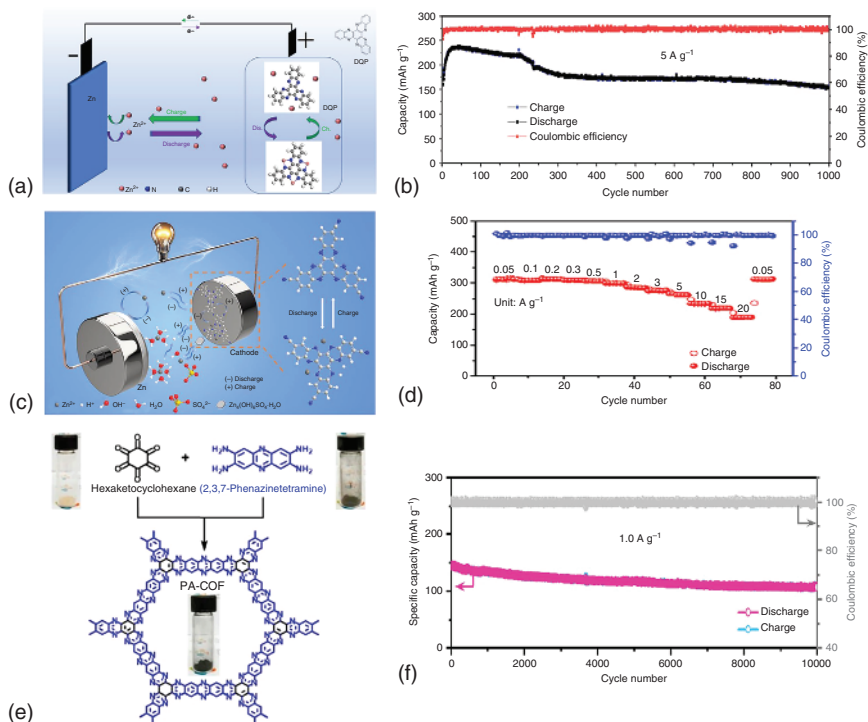
Figure 1.18 (a) Illustration of the working mechanism of DQP//Zn battery. (b) Long-term cycling performance of ZIB based on DQP cathode. Source: Reproduced from Ref. [225]. Copyright 2021, American Chemical Society. (c) Illustration of working mechanism of HATN-3CN//Zn battery. (d) Power density of ZIB based on HATN-3CN cathode. Source: Ye et al. [226], Reproduced with permission from Elsevier. (e) Illustration of the synthetic route of PA-COF. (f) Long-term cycling performance of ZIB based on PA-COF. Source: Wang et al. [227], Reproduced with permission from American Chemical Society, CC BY license.

RZIBs [225]. In order to extend the π-conjugated systems, Ye et al. synthesized a diquinoxalino[2,3-a : 2′,3′-c]phenazine (DQP) by a facile solvothermal reaction, which has six C=N redox-active groups in one DQP molecule and could combine/disconnect with three Zn^{2+} during discharge/charge processes (Figure 1.18a) [225]. The extended large π-conjugated system could strengthen the intermolecular interactions, which facilitated the formation of layer-stacked structure and boosted the diffusion of cations between adjacent layers [225]. The negative charge on N could disperse extended large π-conjugated system, leading to better stabilization of charge state [225]. Thanks to these merits of the sizeable π-conjugated system of DQP, RZIBs showed good power density and long-term cycling performance (Figure 1.18b), which retained a high specific capacity of $162\,mAh\,g^{-1}$ over 1000 cycles at $5\,A\,g^{-1}$ [225].

To further improve the electrochemical performance of DQP, Ye et al. prepared a cyano-containing aromatic Schiff-base (hexaazatrinaphthylene, denoted as HATN-3CN) by introducing -CN groups on the chemical structure of DQP to lower the HOMO)/LUMO energy (Figure 1.18c) [226]. RZIBs with HATN-3CN cathodes

exhibited excellent power density (Figure 1.18d), which could retain 60.7% of the initial capacity (at a current density of $0.05 \, A \, g^{-1}$) at $20 \, A \, g^{-1}$ [226]. RZIBs with HATN-3CN cathodes also showed ultra-stable long-term cycling performance, which could retain 90.7% capacity after 5800 cycles at the current density of $5 \, A \, g^{-1}$ [226]. The long-term cycling stabilities of MIBs based on the above imine compounds are not ideal and could be improved through fabricating PEMs with high molecular weight, leading to less dissolution in aqueous electrolytes.

As one of the most promising candidates of PEMs, COFs have a highly crystalline π-conjugated system, guaranteeing stable chemical structure during long-term operation in both acidic and basic aqueous electrolyte [227]. Alshareef et al. fabricated a novel phenanthroline COF (PA-COF) with rich C=N redox-active groups through a facile solvothermal method (Figure 1.18e) [227]. The thermogravimetric analysis (TGA) and powder X-ray diffraction (PXRD) data confirmed the periodic structure of PA-COF [227]. RZIBs with PA-COF cathode displayed excellent power density at current density ranging from 0.05 to $10 \, A \, g^{-1}$, which could obtain $240 \, mAh \, g^{-1}$ when the current density was switched back to $0.05 \, A \, g^{-1}$ [227]. Furthermore, RZIBs with PA-COF cathodes exhibited ultra-stable long-term cycling performance during 10 000 cycles at $1 \, A \, g^{-1}$ (Figure 1.18f), in which the capacity decayed only 0.38% per cycle, demonstrating the stable chemical structure of PA-COF [227].

1.6 Conclusion and Perspectives

1.6.1 Conclusion

PEMs can be controlled via molecular and morphological engineering to satisfy the requirements of next-generation metal-ion batteries. Firstly, molecular engineering of PEMs can be carried out through grafting of various redox groups, resulting in various types of PEMs such as carbonyl, sulfur-containing, nitrogen-containing, conducting polymers, radical-based, and overlithiation. Molecular engineering also benefits the design and modification of molecular backbones with different functional groups (i.e. electron-withdrawing or -donating) and redox groups, which are closely related to energy density, power density, and cycle life. Secondly, morphological engineering can tailor the interfacial properties of PEMs and electrolytes to form PEMs with 0D, 1D, 2D, and 3D nanostructures through bottom-up (*in situ*) and top-down (*ex situ*) approaches, promoting fast electron conduction and ion diffusion rate, and stable electrode structures. The challenges of low capacity, high solubility, low electronic conductivity, and low stability also can be addressed by fabricating PEMs in various dimensional nanostructure morphologies. This provides effective and inspiring guidance for building high-performance PEMs for practical metal-ion battery applications. Thirdly, applications of PEMs in various advanced rechargeable metal ions such as LIBs, SIBs, KIBs, and multivalent metal-ion batteries have been introduced and discussed thoroughly. The challenges and improvement strategies of PEMs in various metal-ion batteries also have been highlighted and analyzed, which may build a solid foundation for fabricating high-performance rechargeable batteries with PEMs.

1.6.2 Perspectives

Affordable, recyclable, and electrochemically reversible PEMs have shown great potential as energy storage and conversion materials with high capacity, safety, and cost-effectiveness. In this chapter, we identified significant progress in addressing PEMs challenges through molecular and morphological engineering, which may have remarkable impacts on battery performance.

From the perspective of PEMs practical application, strategies that combine PEMs with functional and conductive nanomaterials can be employed to address these challenges during electrode fabrication processes, especially for large-scale applications in rechargeable battery systems with original equipment manufacturers.

(i) The easy dissolution of PEMs in liquid electrolyte remains an inherent disadvantage, especially for PEMs with nanoscale structures. Combining PEMs with functional additives (e.g. polar conductive materials) to generate intramolecular/intermolecular forces (e.g. extended conjugation, mixing with inorganic conductive substrates) can solve/mitigate the parasitic dissolution problems of PEMs [228].

(ii) Low electrical conductivity of PEMs and aggregation of nanostructured PEMs lead to decreased capacity and power density [229–231]. The combination of PEMs with conductive nanomaterials, such as graphene and carbon nanotubes, can prevent aggregation and solve the low conductivity dilemma of PEMs [232, 233].

From the perspective of PEMs design and development, strong theoretical guidance is helpful in improving the PEMs' practicability and efficiency. In order to replace the traditional trial-and-error approach, theoretical and computational chemistry of PEMs can provide us with a range of potential benefits, including the prediction of ideal molecular structures, functional groups and morphological configurations, and even the cost of PEMs. More than 9 million organic compounds and corresponding synthetic methods are a solid statistical basis for artificial intelligence (AI) machine learning. AI is able to extract PEM design, characterization, and electrochemical performances from different publications and other fields, making PEMs' structure and properties easily accessible. In addition, AI can automatically research, design, and optimize novel PEMs with the most straightforward synthesis steps and at the lowest cost. Theoretical models of PEMs can be constructed and run by computational methods (i.e. density functional theory and molecular dynamics) to predict physical properties and battery performances, which have been reported in the literature [234]. Therefore, the widespread application of computational chemistry could accelerate the rollout of the new generation of energy storage PEMs.

From the perspective of possible applications in novel energy storage devices, PEMs can be versatile electrode materials for dual-ion batteries (DIBs) that undergo simultaneous reversible anion intercalation/extraction (e.g. PF_6^-, ClO_4^-, BF^-, and $TFSI^-$) at the cathode and cationic (e.g. Li^+, Na^+, K^+) at the anode. The unique DIBs can significantly improve power density and energy density because they allow simultaneous reactions on both sides of electrodes [235]. PEMs can act as anion-accepting cathode materials in DIBs to replace traditional graphites such

as thianthrene [236], coroene [237], and terephthalate [238]. The unique anion intercalation reaction of the cathode favors high working potential and fast battery kinetics, resulting in improved energy density and power density. High-voltage stable and active PEMs, i.e. p-type radical PEMs and conducting polymers, could store different anions with high capacity and stability according to the redox mechanism of PEMs.

From the perspective of materials characterization and mechanism studies, advanced characterization techniques are essential to obtain material information of PEMs. Mass spectrometry (MS), nuclear magnetic resonance (NMR), Fourier transform infrared spectroscopy (FT-IR), and Raman spectroscopy are common methods to characterize the molecular structure of PEMs. Scanning electron microscopy (SEM) and transmission electron microscopy (TEM) are crucial instruments to investigate the morphological features of PEMs at the microscopic level. In addition to these methods, *in situ* characterization techniques (e.g. *in situ* FT-IR, *in situ* Raman, and *in situ* XRD) have been validated to study the redox mechanisms of PEMs during the charge/discharge processes. More importantly, *in situ* synchrotron X-ray techniques should be another viable option for obtaining sufficient and reliable information on PEMs.

References

1 Li, M., Lu, J., Chen, Z. et al. (2018). 30 years of lithium-ion batteries. *Advanced Materials* 30 (33): 1800561.

2 Whittingham, M.S. (2004). Lithium batteries and cathode materials. *Chemical Reviews* 104 (10): 4271–4302.

3 Cheng, X.B., Zhang, R., Zhao, C.Z. et al. (2017). Toward safe lithium metal anode in rechargeable batteries: a review. *Chemical Reviews* 117 (15): 10403–10473.

4 Vidu, R. and Stroeve, P. (2004). Improvement of the thermal stability of Li-ion batteries by polymer coating of $LiMn_2O_4$. *Industrial & Engineering Chemistry Research* 43 (13): 3314–3324.

5 Yamada, A., Chung, S.C., and Hinokuma, K. (2001). Optimized $LiFePO_4$ for lithium battery cathodes. *Journal of the Electrochemical Society* 148 (3): A224.

6 Li, D.C., Muta, T., Zhang, L.Q. et al. (2004). Effect of synthesis method on the electrochemical performance of $LiNi_{1/3}Mn_{1/3}Co_{1/3}O_2$. *Journal of Power Sources* 132 (1–2): 150–155.

7 Ling, M., Xu, Y.N., Zhao, H. et al. (2015). Dual-functional gum arabic binder for silicon anodes in lithium ion batteries. *Nano Energy* 12: 178–185.

8 Chen, H., Wu, Z.Z., Su, Z. et al. (2021). A mechanically robust self-healing binder for silicon anode in lithium ion batteries. *Nano Energy* 81: 105654.

9 Zhang, L., Wang, C.R., Dou, Y.H. et al. (2019). A yolk–shell structured silicon anode with superior conductivity and high tap density for full lithium-ion batteries. *Angewandte Chemie International Edition* 58 (26): 8824–8828.

10 Liu, T.F., Chu, Q.L., Yan, C. et al. (2019). Interweaving 3D network binder for high-areal-capacity Si anode through combined hard and soft polymers. *Advanced Energy Materials* 9 (3): 1802645.

11 Ling, H.Y., Lai, C., Wang, C.R. et al. (2021). Amylopectin from glutinous rice as a sustainable binder for high-performance silicon anodes. *Energy & Environmental Materials* 4 (2): 263–268.

12 Qian, S.S., Xing, C., Zheng, M.T. et al. (2022). $CuCl_2$-modified lithium metal anode via dynamic protection mechanisms for dendrite-free long-life charging/discharge processes. *Advanced Energy Materials* https://doi.org/10.1002/aenm .202103480.

13 Huang, Y.C., Yang, H., Xiong, T.Z. et al. (2020). Adsorption energy engineering of nickel oxide hybrid nanosheets for high areal capacity flexible lithium-ion batteries. *Energy Storage Materials* 25: 41–51.

14 Ling, H.Y., Chen, H., Wu, Z.Z. et al. (2021). Sustainable bio-derived materials for addressing critical problems of next-generation high-capacity lithium-ion batteries. *Materials Chemistry Frontiers* 5 (16): 5932–5953.

15 Qian, S.S., Chen, H., Wu, Z.Z. et al. (2021). Designing ceramic/polymer composite as highly ionic conductive solid-state electrolytes. *Batteries & Supercaps* 4 (1): 39–59.

16 Chen, H., Adekoya, D., Hencz, L. et al. (2020). Stable seamless interfaces and rapid ionic conductivity of $Ca-CeO_2/LiTfSI/PEO$ composite electrolyte for high-rate and high-voltage all-solid-state battery. *Advanced Energy Materials* 10 (21): 2000049.

17 Chen, H., Ling, M., Hencz, L. et al. (2018). Exploring chemical, mechanical, and electrical functionalities of binders for advanced energy-storage devices. *Chemical Reviews* 118 (18): 8936–8982.

18 Liang, Y.L., Tao, Z.L., and Chen, J. (2012). Organic electrode materials for rechargeable lithium batteries. *Advanced Energy Materials* 2 (7): 742–769.

19 Nishida, S., Yamamoto, Y., Takui, T. et al. (2013). Organic rechargeable batteries with tailored voltage and cycle performance. *ChemSusChem* 6 (5): 794–797.

20 Sun, T., Li, Z.J., Zhi, Y.F. et al. (2021). Poly (2, 5-dihydroxy-1, 4-benzoquinonyl sulfide) as an efficient cathode for high-performance aqueous zinc–organic batteries. *Advanced Functional Materials* 31 (16): 2010049.

21 Guo, Z.W., Ma, Y.Y., Dong, X.L. et al. (2018). An environmentally friendly and flexible aqueous zinc battery using an organic cathode. *Angewandte Chemie International Edition* 57 (36): 11737–11741.

22 Xie, J. and Zhang, Q.C. (2019). Recent progress in multivalent metal (Mg, Zn, Ca, and Al) and metal-ion rechargeable batteries with organic materials as promising electrodes. *Small* 15 (15): 1805061.

23 Yin, X.P., Sarkar, S., Shi, S.S. et al. (2020). Recent progress in advanced organic electrode materials for sodium-ion batteries: synthesis, mechanisms, challenges and perspectives. *Advanced Functional Materials* 30 (11): 1908445.

24 Yu, Q.C., Xue, Z.H., Li, M.C. et al. (2021). Electrochemical activity of nitrogen-containing groups in organic electrode materials and related improvement strategies. *Advanced Energy Materials* 11 (7): 2002523.

25 Xu, D.Y., Liang, M.X., Qi, S. et al. (2021). The progress and prospect of tunable organic molecules for organic lithium-ion batteries. *ACS Nano* 15 (1): 47–80.

26 Xu, S.F., Chen, Y., and Wang, C.L. (2020). Emerging organic potassium-ion batteries: electrodes and electrolytes. *Journal of Materials Chemistry A* 8 (31): 15547–15574.

27 Chen, Y., Zhuo, S.M., Li, Z.Y. et al. (2020). Redox polymers for rechargeable metal-ion batteries. *EnergyChem* 2 (2): 100030.

28 Rajagopalan, R., Tang, Y.G., Jia, C.K. et al. (2020). Understanding the sodium storage mechanisms of organic electrodes in sodium ion batteries: issues and solutions. *Energy & Environmental Science* 13 (6): 1568–1592.

29 Williams, D.L., Byrne, J.J., and Driscoll, J.S. (1969). A high energy density lithium/dichloroisocyanuric acid battery system. *Journal of the Electrochemical Society* 116 (1): 2.

30 Wang, G., Chandrasekhar, N., Biswal, B.P. et al. (2019). A crystalline, 2D polyarylimide cathode for ultrastable and ultrafast Li storage. *Advanced Materials* 31 (28): 1901478.

31 Song, Z.P., Qian, Y.M., Gordin, M.L. et al. (2015). Polyanthraquinone as a reliable organic electrode for stable and fast lithium storage. *Angewandte Chemie International Edition* 127 (47): 14153–14157.

32 Lu, Y., Hou, X.S., Miao, L.C. et al. (2019). Cyclohexanehexone with ultrahigh capacity as cathode materials for lithium-ion batteries. *Angewandte Chemie International Edition* 58 (21): 7020–7024.

33 Zhao, Q., Huang, W.W., Luo, Z.Q. et al. (2018). High-capacity aqueous zinc batteries using sustainable quinone electrodes. *Science Advances* 4 (3): eaao1761.

34 Huang, W.W., Zheng, S.B., Zhang, X.Q. et al. (2020). Synthesis and application of calix[6]quinone as a high-capacity organic cathode for plastic crystal electrolyte-based lithium-ion batteries. *Energy Storage Materials* 26: 465–471.

35 Jouhara, A., Dupré, N., Gaillot, A.C. et al. (2018). Raising the redox potential in carboxyphenolate-based positive organic materials via cation substitution. *Nature Communications* 9 (1): 4401.

36 Lee, M., Hong, J., Lopez, J. et al. (2017). High-performance sodium–organic battery by realizing four-sodium storage in disodium rhodizonate. *Nature Energy* 2 (11): 861–868.

37 Armand, M., Grugeon, S., Vezin, H. et al. (2009). Conjugated dicarboxylate anodes for Li-ion batteries. *Nature Materials* 8 (2): 120–125.

38 Peng, H.L., Yu, Q.C., Wang, S.P. et al. (2019). Molecular design strategies for electrochemical behavior of aromatic carbonyl compounds in organic and aqueous electrolytes. *Advanced Science* 6 (17): 1900431.

39 Yang, J.X., Xiong, P.X., Shi, Y.Q. et al. (2020). Rational molecular design of benzoquinone-derived cathode materials for high-performance lithium-ion batteries. *Advanced Functional Materials* 30 (15): 1909597.

40 Luo, Z.Q., Liu, L.J., Zhao, Q. et al. (2017). An insoluble benzoquinone-based organic cathode for use in rechargeable lithium-ion batteries. *Angewandte Chemie International Edition* 56 (41): 12561–12565.

41 Pan, Q.G., Zheng, Y.P., Tong, Z.P. et al. (2021). Novel lamellar tetrapotassium pyromellitic organic for robust high-capacity potassium storage. *Angewandte Chemie International Edition* 60 (21): 11835–11840.

42 Luo, C., Shea, J.J., and Huang, J.H. (2020). A carboxylate group-based organic anode for sustainable and stable sodium ion batteries. *Journal of Power Sources* 453: 227904.

43 Ma, C., Zhao, X.L., Kang, L.T. et al. (2018). Non-conjugated dicarboxylate anode materials for electrochemical cells. *Angewandte Chemie International Edition* 57 (29): 8865–8870.

44 Perticarari, S., Doizy, T., Soudan, P. et al. (2019). Intermixed cation–anion aqueous battery based on an extremely fast and long-cycling di-block bipyridinium–naphthalene diimide oligomer. *Advanced Energy Materials* 9 (25): 1803688.

45 Ruby, R.M., Mangalaraja, R.V., Contreras, D. et al. (2020). Perylenedianhydride-based polyimides as organic cathodes for rechargeable lithium and sodium batteries. *ACS Applied Energy Materials* 3 (1): 240–252.

46 Wang, X.S., Chen, L., Lu, F. et al. (2019). Boosting aqueous Zn^{2+} storage in 1,4,5,8-naphthalenetetracarboxylic dianhydride through nitrogen substitution. *ChemElectroChem* 6 (14): 3644–3647.

47 Wang, X.F., Bommier, C., Jian, Z.L. et al. (2017). Hydronium-ion batteries with perylenetetracarboxylic dianhydride crystals as an electrode. *Angewandte Chemie International Edition* 56 (11): 2909–2913.

48 Oubaha, H., Gohy, J.F., and Melinte, S. (2019). Carbonyl-based π-conjugated materials: from synthesis to applications in lithium-ion batteries. *ChemPlusChem* 84 (9): 1179–1214.

49 Zhang, K., Guo, C.Y., Zhao, Q. et al. (2015). High-performance organic lithium batteries with an ether-based electrolyte and 9,10-anthraquinone (aq)/CMK-3 cathode. *Advanced Science* 2 (5): 1500018.

50 Bitenc, J., Lindahl, N., Vizintin, A. et al. (2020). Concept and electrochemical mechanism of an al metal anode–organic cathode battery. *Energy Storage Materials* 24: 379–383.

51 Shadike, Z., Tan, S., Wang, Q.C. et al. (2021). Review on organosulfur materials for rechargeable lithium batteries. *Materials Horizons* 8 (2): 471–500.

52 Zhang, X.Y., Chen, K., Sun, Z.H. et al. (2020). Structure-related electrochemical performance of organosulfur compounds for lithium–sulfur batteries. *Energy & Environmental Science* 13 (4): 1076–1095.

53 Wang, D.Y., Guo, W., and Fu, Y.Z. (2019). Organosulfides: an emerging class of cathode materials for rechargeable lithium batteries. *Accounts of Chemical Research* 52 (8): 2290–2300.

54 Visco, S.J. and DeJonghe, L.C. (1988). Ionic conductivity of organosulfur melts for advanced storage electrodes. *Journal of the Electrochemical Society* 135 (12): 2905.

55 Wang, D.Y., Si, Y.B., Li, J.J. et al. (2019). Tuning the electrochemical behavior of organodisulfides in rechargeable lithium batteries using N-containing heterocycles. *Journal of Materials Chemistry A* 7 (13): 7423–7429.

56 NuLi, Y., Guo, Z.P., Liu, H.K. et al. (2007). A new class of cathode materials for rechargeable magnesium batteries: organosulfur compounds based on sulfur–sulfur bonds. *Electrochemistry Communications* 9 (8): 1913–1917.

57 Song, Z.P. and Zhou, H.S. (2013). Towards sustainable and versatile energy storage devices: an overview of organic electrode materials. *Energy & Environmental Science* 6 (8): 2280–2301.

58 Peng, C.X., Ning, G.H., Jie, S. et al. (2017). Reversible multi-electron redox chemistry of π-conjugated N-containing heteroaromatic molecule-based organic cathodes. *Nature Energy* 2 (7): 17074.

59 Mao, M., Luo, C., Pollard, T.P. et al. (2019). A pyrazine-based polymer for fast-charge batteries. *Angewandte Chemie International Edition* 58 (49): 17820–17826.

60 López-Herraiz, M., Castillo-Martínez, E., Carretero-González, J. et al. (2015). Oligomeric-schiff bases as negative electrodes for sodium ion batteries: unveiling the nature of their active redox centers. *Energy & Environmental Science* 8 (11): 3233–3241.

61 Castillo-Martinez, E., Carretero-Gonzalez, J., and Armand, M. (2014). Polymeric schiff bases as low-voltage redox centers for sodium-ion batteries. *Angewandte Chemie International Edition* 53 (21): 5341–5345.

62 Lin, Z.Q., Xie, J., Zhang, B.W. et al. (2017). Solution-processed nitrogen-rich graphene-like holey conjugated polymer for efficient lithium ion storage. *Nano Energy* 41: 117–127.

63 Sakaushi, K., Hosono, E., Nickerl, G. et al. (2013). Aromatic porous-honeycomb electrodes for a sodium-organic energy storage device. *Nature Communications* 4 (1): 1485.

64 Eder, S., Yoo, D.J., Nogala, W. et al. (2020). Switching between local and global aromaticity in a conjugated macrocycle for high-performance organic sodium-ion battery anodes. *Angewandte Chemie International Edition* 59 (31): 12958–12964.

65 Hong, J., Lee, M., Lee, B. et al. (2014). Biologically inspired pteridine redox centres for rechargeable batteries. *Nature Communications* 5 (1): 5335.

66 Tobishima, S., Yamaki, J., and Yamaji, A. (1984). Cathode characteristics of organic electron acceptors for lithium batteries. *Journal of the Electrochemical Society* 131 (1): 57–63.

67 Deng, Q.J., He, S.J., Pei, J.F. et al. (2017). Exploitation of redox-active 1,4-dicyanobenzene and 9,10-dicyanoanthracene as the organic electrode materials in rechargeable lithium battery. *Electrochemistry Communications* 75: 29–32.

68 Luo, C., Ji, X., Hou, S. et al. (2018). Azo compounds derived from electro-chemical reduction of nitro compounds for high performance Li-ion batteries. *Advanced Materials* 30 (23): 1706498.

69 Luo, C., Borodin, O., Ji, X. et al. (2018). Azo compounds as a family of organic electrode materials for alkali-ion batteries. *Proceedings of the National Academy of Science* 115 (9): 2004–2009.

70 Zhang, C., Yang, X., Ren, W.F. et al. (2016). Microporous organic polymer-based lithium ion batteries with improved rate performance and energy density. *Journal of Power Sources* 317: 49–56.

71 Obrezkov, F.A., Shestakov, A.F., Traven, V.F. et al. (2019). An ultrafast charging polyphenylamine-based cathode material for high rate lithium, sodium and potassium batteries. *Journal of Materials Chemistry A* 7 (18): 11430–11437.

72 Deng, W.W., Liang, X.M., Wu, X.Y. et al. (2013). A low cost, all-organic na-ion battery based on polymeric cathode and anode. *Scientific Reports* 3 (1): 2671.

73 Nigrey, P.J., Macinnes, D., Nairns, D.P. et al. (1981). Lightweight rechargeable storage batteries using polyacetylene, $(CH)_x$ as the cathode-active material. *Journal of the Electrochemical Society* 128 (8): 1651–1654.

74 Jia, X.T., Ge, Y., Shao, L. et al. (2019). Tunable conducting polymers: toward sustainable and versatile batteries. *ACS Sustainable Chemistry & Engineering* 7 (17): 14321–14340.

75 Wan, F., Zhang, L.L., Wang, X.Y. et al. (2018). An aqueous rechargeable zinc-organic battery with hybrid mechanism. *Advanced Functional Materials* 28 (45): 1804975.

76 Han, C.P., Tong, J., Tang, X. et al. (2020). Boost anion storage capacity using conductive polymer as a pseudocapacitive cathode for high-energy and flexible lithium ion capacitors. *ACS Applied Materials & Interfaces* 12 (9): 10479–10489.

77 Wu, Y.C., Chen, Y., Tang, M. et al. (2019). A highly conductive conjugated coordination polymer for fast-charge sodium-ion batteries: reconsidering its structures. *Chemical Communications* 55 (73): 10856–10859.

78 Shi, Y., Peng, L.L., Ding, Y. et al. (2015). Nanostructured conductive polymers for advanced energy storage. *Chemical Society Reviews* 44 (19): 6684–6696.

79 Shinozaki, K., Tomizuka, Y., and Nojiri, A. (1984). Performance of lithium/polyacetylene cell. *Japanese Journal of Applied Physics* 23 (12): L892–L894.

80 Nakahara, K., Iwasa, S., Satoh, M. et al. (2002). Rechargeable batteries with organic radical cathodes. *Chemical Physics Letters* 359 (5–6): 351–354.

81 Oyaizu, K. and Nishide, H. (2009). Radical polymers for organic electronic devices: a radical departure from conjugated polymers? *Advanced Materials* 21 (22): 2339–2344.

82 Lu, Y., Zhang, Q., Li, L. et al. (2018). Design strategies toward enhancing the performance of organic electrode materials in metal-ion batteries. *Chem* 4 (12): 2786–2813.

83 Renault, S., Oltean, V.A., Araujo, C.M. et al. (2016). Superlithiation of organic electrode materials: the case of dilithium benzenedipropiolate. *Chemistry of Materials* 28 (6): 1920–1926.

84 Wang, J., Yao, H.Y., Du, C.Y. et al. (2021). Polyimide schiff base as a high-performance anode material for lithium-ion batteries. *Journal of Power Sources* 482: 228931.

85 Han, X.Y., Qing, G.Y., Sun, J.T. et al. (2012). How many lithium ions can be inserted onto fused C6 aromatic ring systems? *Angewandte Chemie International Edition* 124 (21): 5237–5241.

86 Li, G.P., Zhang, B.J., Wang, J.W. et al. (2019). Electrochromic poly(chalcogenoviologen)s as anode materials for high-performance organic radical lithium-ion batteries. *Angewandte Chemie International Edition* 58 (25): 8468–8473.

87 Man, Z.M., Li, P., Zhou, D. et al. (2019). High-performance lithium–organic batteries by achieving 16 lithium storage in poly(imine-anthraquinone). *Journal of Materials Chemistry A* 7 (5): 2368–2375.

88 Kang, H.W., Liu, H.L., Li, C.X. et al. (2018). Polyanthraquinone-triazine—a promising anode material for high-energy lithium-ion batteries. *ACS Applied Materials & Interfaces* 10 (43): 37023–37030.

89 Yang, H.Q., Liu, S.W., Cao, L.H. et al. (2018). Superlithiation of non-conductive polyimide toward high-performance lithium-ion batteries. *Journal of Materials Chemistry A* 6 (42): 21216–21224.

90 Sun, T., Li, Z.J., Wang, H.G. et al. (2016). A biodegradable polydopamine-derived electrode material for high-capacity and long-life lithium-ion and sodium-ion batteries. *Angewandte Chemie International Edition* 55 (36): 10662–10666.

91 Wu, J.S., Rui, X.H., Long, G.K. et al. (2015). Pushing up lithium storage through nanostructured polyazaacene analogues as anode. *Angewandte Chemie International Edition* 54 (25): 7354–7358.

92 Zhao, L.B., Gao, S.T., He, R.X. et al. (2018). Molecular design of phenan-threnequinone derivatives as organic cathode materials. *ChemSusChem* 11 (7): 1215–1222.

93 Jung, K.H., Jeong, G.S., Go, C.Y. et al. (2020). Conjugacy of organic cathode materials for high-potential lithium-ion batteries: carbonitriles versus quinones. *Energy Storage Materials* 24: 237–246.

94 Morita, Y., Nishida, S., Murata, T. et al. (2011). Organic tailored batteries materials using stable open-shell molecules with degenerate frontier orbitals. *Nature Materials* 10 (12): 947–951.

95 Lee, M., Hong, J., Seo, D.H. et al. (2013). Redox cofactor from biological energy transduction as molecularly tunable energy-storage compound. *Angewandte Chemie International Edition* 52 (32): 8322–8328.

96 Kim, H., Kwon, J.E., Lee, B. et al. (2015). High energy organic cathode for sodium rechargeable batteries. *Chemistry of Materials* 27 (21): 7258–7264.

97 Park, Y., Shin, D.S., Woo, S.H. et al. (2012). Sodium terephthalate as an organic anode material for sodium ion batteries. *Advanced Materials* 24 (26): 3562–3567.

98 Banda, H. and D.D., Nagarajan K., et al. (2017). Twisted perylene diimides with tunable redox properties for organic sodium-ion batteries. *Advanced Energy Materials* 7 (20): 1701316.

99 Vadehra, G.S., Maloney, R.P., Garcia-Garibay, M.A. et al. (2014). Naphthalene diimide based materials with adjustable redox potentials: evaluation for organic lithium-ion batteries. *Chemistry of Materials* 26 (24): 7151–7157.

100 Lyu, H., Jafta, C.J., Popovs, I. et al. (2019). A dicyanobenzoquinone based cathode material for rechargeable lithium and sodium ion batteries. *Journal of Materials Chemistry A* 7 (30): 17888–17895.

101 Wan, W., Lee, H., Yu, X.Q. et al. (2014). Tuning the electrochemical performances of anthraquinone organic cathode materials for li-ion batteries through the sulfonic sodium functional group. *RSC Advances* 4 (38): 19878–19882.

102 Lu, Y., Zhao, Q., Miao, L.C. et al. (2017). Flexible and free-standing organic/carbon nanotubes hybrid films as cathode for rechargeable lithium-ion batteries. *The Journal of Physical Chemistry C* 121 (27): 14498–14506.

103 Liang, Y.L., Zhang, P., and Chen, J. (2013). Function-oriented design of conjugated carbonyl compound electrodes for high energy lithium batteries. *Chemical Science* 4 (3): 1330–1337.

104 Liang, Y.L., Zhang, P., Yang, S.Q. et al. (2013). Fused heteroaromatic organic compounds for high-power electrodes of rechargeable lithium batteries. *Advanced Energy Materials* 3 (5): 600–605.

105 Burkhardt, S.E., Lowe, M.A., Conte, S. et al. (2012). Tailored redox functionality of small organics for pseudocapacitive electrodes. *Energy & Environmental Science* 5 (5): 7176–7187.

106 Heiska, J., Nisula, M., and Karppinen, M. (2019). Organic electrode materials with solid-state battery technology. *Journal of Materials Chemistry A* 7 (32): 18735–18758.

107 Lee, J. and Park, M.J. (2017). Tattooing dye as a green electrode material for lithium batteries. *Advanced Energy Materials* 7 (12): 1602279.

108 Liang, Y., Jing, Y., Gheytani, S. et al. (2017). Universal quinone electrodes for long cycle life aqueous rechargeable batteries. *Nature Materials* 16 (8): 841–848.

109 Zhao, H.Y., Wang, J.W., Zheng, Y.H. et al. (2017). Organic thiocarboxylate electrodes for a room-temperature sodium-ion battery delivering an ultrahigh capacity. *Angewandte Chemie International Edition* 56 (48): 15334–15338.

110 Lu, Y. and Chen, J. (2020). Prospects of organic electrode materials for practical lithium batteries. *Nature Reviews Chemistry* 4 (3): 127–142.

111 Lee, J., Kim, H., and Park, M.J. (2016). Long-life, high-rate lithium-organic batteries based on naphthoquinone derivatives. *Chemistry of Materials* 28 (7): 2408–2416.

112 Liang, Y.L., Chen, Z.H., Jing, Y. et al. (2015). Heavily N-dopable π-conjugated redox polymers with ultrafast energy storage capability. *Journal of the American Chemical Society* 137 (15): 4956–4959.

113 Acker, P., Rzesny, L., Marchiori Cleber, F.N. et al. (2019). π-conjugation enables ultra-high rate capabilities and cycling stabilities in phenothiazine copolymers as cathode-active battery materials. *Advanced Functional Materials* 29 (45): 1906436.

114 Gao, X., Chen, Y., Gu, C.J. et al. (2020). Non-conjugated diketone as a linkage for enhancing the rate performance of poly(perylenediimides). *Journal of Materials Chemistry A* 8 (37): 19283–19289.

115 Xue, J., Fan, C., Deng, Q.J. et al. (2016). Silver terephthalate ($Ag_2C_8H_4O_4$) offering in-situ formed metal/organic nanocomposite as the highly efficient organic anode in Li-ion and Na-ion batteries. *Electrochimica Acta* 219: 418–424.

116 Shimizu, A., Kuramoto, H., Tsujii, Y. et al. (2014). Introduction of two lithiooxycarbonyl groups enhances cyclability of lithium batteries with organic cathode materials. *Journal of Power Sources* 260: 211–217.

117 Yokoji, T., Kameyama, Y., Maruyama, N. et al. (2016). High-capacity organic cathode active materials of 2,2′-bis-p-benzoquinone derivatives for rechargeable batteries. *Journal of Materials Chemistry A* 4 (15): 5457–5466.

118 Song, Z.P., Qian, Y.M., Zhang, T. et al. (2015). Poly(benzoquinonyl sulfide) as a high-energy organic cathode for rechargeable li and na batteries. *Advanced Science* 2 (9): 1500124.

119 Zheng, J., Wu, Y., Sun, Y. et al. (2020). Advanced anode materials of potassium ion batteries: from zero dimension to three dimensions. *Nano-Micro Letters* 13 (1): 12.

120 Pham, T.N., Park, D., Lee, Y. et al. (2019). Combination-based nanomaterial designs in single and double dimensions for improved electrodes in lithium ion-batteries and faradaic supercapacitors. *Journal of Energy Chemistry* 38: 119–146.

121 Zhuo, S.M., Tang, M., Wu, Y.C. et al. (2019). Size control of zwitterionic polymer micro/nanospheres and its dependence on sodium storage. *Nanoscale Horizons* 4 (5): 1092–1098.

122 Luo, C., Huang, R., Kevorkyants, R. et al. (2014). Self-assembled organic nanowires for high power density lithium ion batteries. *Nano Letters* 14 (3): 1596–1602.

123 Kong, L.J., Liu, M., Huang, H. et al. (2021). Metal/covalent-organic framework based cathodes for metal-ion batteries. *Advanced Energy Materials* 12 (4): 2100172.

124 Lim, S.A. and Ahmed, M.U. (2016). Electrochemical immunosensors and their recent nanomaterial-based signal amplification strategies: a review. *RSC Advances* 6 (30): 24995–25014.

125 Gannett, C.N., Melecio-Zambrano, L., Theibault, M.J. et al. (2021). Organic electrode materials for fast-rate, high-power battery applications. *Materials Reports: Energy* 1 (1): 100008.

126 Xu, Y., Zhou, M., and Lei, Y. (2018). Organic materials for rechargeable sodium-ion batteries. *Materials Today* 21 (1): 60–78.

127 Patra, B.C., Das, S.K., Ghosh, A. et al. (2018). Covalent organic framework based microspheres as an anode material for rechargeable sodium batteries. *Journal of Materials Chemistry A* 6 (34): 16655–16663.

128 Li, Z.P., Zhong, W.H., Cheng, A. et al. (2018). Novel hyper-crosslinked polymer anode for lithium-ion batteries with highly reversible capacity and long cycling stability. *Electrochimica Acta* 281: 162–169.

129 Xu, F., Chen, X., Tang, Z.W. et al. (2014). Redox-active conjugated microporous polymers: a new organic platform for highly efficient energy storage. *Chemical Communications* 50 (37): 4788–4790.

130 Lu, A.H., Hao, G.P., Sun, Q. et al. (2012). Chemical synthesis of carbon materials with intriguing nanostructure and morphology. *Macromolecular Chemistry and Physics* 213 (10–11): 1107–1131.

131 Wang, C.L. (2020). Weak intermolecular interactions for strengthening organic batteries. *Energy & Environmental Materials* 3 (4): 441–452.

132 Rani, A., Reddy, R., Sharma, U. et al. (2018). A review on the progress of nanostructure materials for energy harnessing and environmental remediation. *Journal of Nanostructure in Chemistry* 8 (3): 255–291.

133 Deng, W., Shen, Y., Qian, J. et al. (2015). A perylene diimide crystal with high capacity and stable cyclability for Na-ion batteries. *ACS Applied Materials & Interfaces* 7 (38): 21095–21099.

134 See, K.A., Hug, S., Schwinghammer, K. et al. (2015). Lithium charge storage mechanisms of cross-linked triazine networks and their porous carbon derivatives. *Chemistry of Materials* 27 (11): 3821–3829.

135 Pomerantseva, E., Bonaccorso, F., Feng, X. et al. (2019). Energy storage: the future enabled by nanomaterials. *Science* 366 (6468): eaan8285.

136 Lee, M., Hong, J., Kim, H. et al. (2014). Organic nanohybrids for fast and sustainable energy storage. *Advanced Materials* 26 (16): 2558–2565.

137 Wang, S., Wang, L., Zhu, Z. et al. (2014). All organic sodium-ion batteries with Na(4)C(8)H(2)O(6). *Angewandte Chemie International Edition* 53 (23): 5892–5896.

138 Ba, Z., Wang, Z., Luo, M. et al. (2020). Benzoquinone-based polyimide derivatives as high-capacity and stable organic cathodes for lithium-ion batteries. *ACS Applied Materials & Interfaces* 12 (1): 807–817.

139 Banda, H., Damien, D., Nagarajan, K. et al. (2015). A polyimide based all-organic sodium ion battery. *Journal of Materials Chemistry A* 3 (19): 10453–10458.

140 Xu, S.Q., Wang, G., Biswal, B.P. et al. (2019). A nitrogen-rich 2D sp^2-carbon-linked conjugated polymer framework as a high-performance cathode for lithium-ion batteries. *Angewandte Chemie International Edition* 58 (3): 849–853.

141 Sun, T., Xie, J., Guo, W. et al. (2020). Covalent–organic frameworks: Advanced organic electrode materials for rechargeable batteries. *Advanced Energy Materials* 10 (19): 1904199.

142 Byeon, H., Gu, B., Kim, H.J. et al. (2021). Redox chemistry of nitrogen-doped cnt-encapsulated nitroxide radical polymers for high energy density and rate-capability organic batteries. *Chemical Engineering Journal* 413: 127402.

143 Kim, J.K., Kim, Y., Park, S. et al. (2016). Encapsulation of organic active materials in carbon nanotubes for application to high-electrochemical-performance sodium batteries. *Energy & Environmental Science* 9 (4): 1264–1269.

144 Wang, Y., Ding, Y., Pan, L. et al. (2016). Understanding the size-dependent sodium storage properties of $Na_2C_6O_6$-based organic electrodes for sodium-ion batteries. *Nano Letters* 16 (5): 3329–3334.

145 Kim, J.K., Scheers, J., Ahn, J.H. et al. (2013). Nano-fibrous polymer films for organic rechargeable batteries. *Journal of Materials Chemistry A* 1 (7): 2426–2430.

146 Schon, T.B., McAllister, B.T., Li, P.F. et al. (2016). The rise of organic electrode materials for energy storage. *Chemical Society Reviews* 45 (22): 6345–6404.

147 Yong, B., Ma, D.T., Wang, Y.Y. et al. (2020). Understanding the design principles of advanced aqueous zinc-ion battery cathodes: from transport kinetics to structural engineering, and future perspectives. *Advanced Energy Materials* 10 (45): 2002354.

148 Xie, J., Gu, P.Y., and Zhang, Q.C. (2017). Nanostructured conjugated polymers: toward high-performance organic electrodes for rechargeable batteries. *ACS Energy Letters* 2 (9): 1985–1996.

149 Yang, H., Zhang, S., Han, L. et al. (2016). High conductive two-dimensional covalent organic framework for lithium storage with large capacity. *ACS Applied Materials & Interfaces* 8 (8): 5366–5375.

150 Luo, Z., Liu, L., Ning, J. et al. (2018). A microporous covalent-organic framework with abundant accessible carbonyl groups for lithium-ion batteries. *Angewandte Chemie International Edition* 57 (30): 9443–9446.

151 Gu, S., Wu, S., Cao, L. et al. (2019). Tunable redox chemistry and stability of radical intermediates in 2D covalent organic frameworks for high performance sodium ion batteries. *Journal of the American Chemical Society* 141 (24): 9623–9628.

152 Chen, X.D., Sun, W.W., and Wang, Y. (2020). Covalent organic frameworks for next-generation batteries. *ChemElectroChem* 7 (19): 3905–3926.

153 Shi, R.J., Liu, L.J., Lu, Y. et al. (2020). Nitrogen-rich covalent organic frameworks with multiple carbonyls for high-performance sodium batteries. *Nature Communications* 11 (1): 178.

154 Meng, L., Ren, S., Ma, C. et al. (2019). Synthesis of a 2D nitrogen-rich pi-conjugated microporous polymer for high performance lithium-ion batteries. *Chemical Communications* 55 (64): 9491–9494.

155 Haldar, S., Roy, K., Nandi, S. et al. (2018). High and reversible lithium ion storage in self-exfoliated triazole-triformyl phloroglucinol-based covalent organic nanosheets. *Advanced Energy Materials* 8 (8): 1702170.

156 Kim, M.S., Lee, W.J., Paek, S.M. et al. (2018). Covalent organic nanosheets as effective sodium-ion storage materials. *ACS Applied Materials & Interfaces* 10 (38): 32102–32111.

157 Wang, Y., Li, X.L., Chen, L. et al. (2019). Ultrahigh-capacity tetrahydroxybenzo-quinone grafted graphene material as a novel anode for lithium-ion batteries. *Carbon* 155: 445–452.

158 Wan, F., Wu, X.L., Guo, J.Z. et al. (2015). Nanoeffects promote the electro-chemical properties of organic $Na_2C_8H_4O_4$ as anode material for sodium-ion batteries. *Nano Energy* 13: 450–457.

159 Kong, L., Zhong, M., Shuang, W. et al. (2020). Electrochemically active sites inside crystalline porous materials for energy storage and conversion. *Chemical Society Reviews* 49 (8): 2378–2407.

160 Singh, H., Devi, M., Jena, N. et al. (2020). Proton-triggered fluorescence switching in self-exfoliated ionic covalent organic nanosheets for applications in selective detection of anions. *ACS Applied Materials & Interfaces* 12 (11): 13248–13255.

161 Mitra, S., Kandambeth, S., Biswal, B.P. et al. (2016). Self-exfoliated guanidinium-based ionic covalent organic nanosheets (icons). *Journal of the American Chemical Society* 138 (8): 2823–2828.

162 Zhang, N., Wang, T.S., Wu, X. et al. (2018). Self-exfoliation of 2D covalent organic frameworks: morphology transformation induced by solvent polarity. *RSC Advances* 8 (7): 3803–3808.

163 Mal, A., Mishra, R.K., Praveen, V.K. et al. (2018). Supramolecular reassembly of self-exfoliated ionic covalent organic nanosheets for label-free detection of double-stranded DNA. *Angewandte Chemie International Edition* 57 (28): 8443–8447.

164 Zhu, Y., Chen, X., Cao, Y. et al. (2019). Reversible intercalation and exfoliation of layered covalent triazine frameworks for enhanced lithium ion storage. *Chemical Communications* 55 (10): 1434–1437.

165 Zhao, G.F., Li, H.N., Gao, Z.H. et al. (2021). Dual-active-center of polyimide and triazine modified atomic-layer covalent organic frameworks for high-performance Li storage. *Advanced Functional Materials* 31 (29): 2101019.

166 Wang, S., Wang, Q.Y., Shao, P.P. et al. (2017). Exfoliation of covalent organic frameworks into few-layer redox-active nanosheets as cathode materials for lithium-ion batteries. *Journal of the American Chemical Society* 139 (12): 4258–4261.

167 Haldar, S., Roy, K., Kushwaha, R. et al. (2019). Chemical exfoliation as a controlled route to enhance the anodic performance of cof in LIB. *Advanced Energy Materials* 9 (48): 1902428.

168 Wang, S., Wang, L., Zhang, K. et al. (2013). Organic $Li_4C_8H_2O_6$ nanosheets for lithium-ion batteries. *Nano Letters* 13 (9): 4404–4409.

169 Chen, Y. and Wang, C.L. (2020). Designing high performance organic batteries. *Accounts of Chemical Research* 53 (11): 2636–2647.

170 Liu, T.Y., Kim, K.C., Lee, B. et al. (2017). Self-polymerized dopamine as an organic cathode for Li- and Na-ion batteries. *Energy & Environmental Science* 10 (1): 205–215.

171 Molina, A., Patil, N., Ventosa, E. et al. (2020). Electrode engineering of redox-active conjugated microporous polymers for ultra-high areal capacity organic batteries. *ACS Energy Letters* 5 (9): 2945–2953.

172 Han, C.P., Li, H.F., Shi, R.Y. et al. (2019). Organic quinones towards advanced electrochemical energy storage: recent advances and challenges. *Journal of Materials Chemistry A* 7 (41): 23378–23415.

173 Wu, H., Meng, Q., Yang, Q. et al. (2015). Large-area polyimide/swcnt nanocable cathode for flexible lithium-ion batteries. *Advanced Materials* 27 (41): 6504–6510.

174 Hu, Y., Ding, H., Bai, Y. et al. (2019). Rational design of a polyimide cathode for a stable and high-rate potassium-ion battery. *ACS Applied Materials & Interfaces* 11 (45): 42078–42085.

175 Ma, J., Kong, Y., Luo, Y. et al. (2021). Flexible polyimide nanorod/graphene framework as an organic cathode for rechargeable sodium-ion batteries. *The Journal of Physical Chemistry C* 125 (12): 6564–6569.

176 Lyu, H., Li, P., Liu, J. et al. (2018). Aromatic polyimide/graphene composite organic cathodes for fast and sustainable lithium-ion batteries. *ChemSusChem* 11 (4): 763–772.

177 Zhao, J.H., Kang, T., Chu, Y.L. et al. (2019). A polyimide cathode with superior stability and rate capability for lithium-ion batteries. *Nano Research* 12 (6): 1355–1360.

178 Patil, N., Mavrandonakis, A., Jérôme, C. et al. (2021). High-performance all-organic aqueous batteries based on a poly(imide) anode and poly(catechol) cathode. *Journal of Materials Chemistry A* 9 (1): 505–514.

179 Liu, N., Wu, X., Zhang, Y. et al. (2020). Building high rate capability and ultrastable dendrite-free organic anode for rechargeable aqueous zinc batteries. *Advanced Science* 7 (14): 2000146.

180 Amin, K., Meng, Q., Ahmad, A. et al. (2018). A carbonyl compound-based flexible cathode with superior rate performance and cyclic stability for flexible lithium-ion batteries. *Advanced Materials* 30 (4): 1703868.

181 Patil, N., Aqil, A., Ouhib, F. et al. (2017). Bioinspired redox-active catechol-bearing polymers as ultrarobust organic cathodes for lithium storage. *Advanced Materials* 29 (40): 1703373.

182 Jing, B.B. and Evans, C.M. (2019). Catalyst-free dynamic networks for recyclable, self-healing solid polymer electrolytes. *Journal of the American Chemical Society* 141 (48): 18932–18937.

183 Adekoya, D., Qian, S.S., Gu, X.X. et al. (2021). DFT-guided design and fabrication of carbon-nitride-based materials for energy storage devices: a review. *Nano-Micro Letters* 13 (1): 44.

184 Huang, Q., Turcheniuk, K., Ren, X. et al. (2019). Cycle stability of conversion-type iron fluoride lithium battery cathode at elevated temperatures in polymer electrolyte composites. *Nature Materials* 18 (12): 1343–1349.

185 Chen, H., Zheng, M.T., Qian, S.S. et al. (2021). Functional additives for solid polymer electrolytes in flexible and high-energy-density solid-state lithium-ion batteries. *Carbon Energy* 3 (6): 929–956.

186 Gu, X.X., Wang, Y.Z., Lai, C. et al. (2015). Microporous bamboo biochar for lithium-sulfur batteries. *Nano Research* 8 (1): 129–139.

187 Chen, R., Li, Q., Yu, X. et al. (2019). Approaching practically accessible solid-state batteries: stability issues related to solid electrolytes and interfaces. *Chemical Reviews* 120 (14): 6820–6877.

188 Zhao, C.L., Liu, L.L., Qi, X.G. et al. (2018). Solid-state sodium batteries. *Advanced Energy Materials* 8 (17): 1703012.

189 Liu, H., Cheng, X.B., Huang, J.Q. et al. (2020). Controlling dendrite growth in solid-state electrolytes. *ACS Energy Letters* 5 (3): 833–843.

190 Gao, H., Zhu, Q., Neale, A.R. et al. (2021). Integrated covalent organic framework/carbon nanotube composite as li-ion positive electrode with ultra-high rate performance. *Advanced Energy Materials* 11 (39): 2101880.

191 Wu, M.S., Luu Nhu, T.H., Chen, T.H. et al. (2021). Supramolecular self-assembled multi-electron-acceptor organic molecule as high-performance cathode material for li-ion batteries. *Advanced Energy Materials* 11 (31): 2100330.

192 Hu, P., He, X., Ng, M.F. et al. (2019). Trisulfide-bond acenes for organic batteries. *Angewandte Chemie International Edition* 58 (38): 13513–13521.

193 Xu, S., Wang, G., Biswal, B.P. et al. (2019). A nitrogen-rich 2D sp(2) -carbon-linked conjugated polymer framework as a high-performance cathode for lithium-ion batteries. *Angewandte Chemie International Edition* 58 (3): 849–853.

194 Hansen, K.A., Nerkar, J., Thomas, K. et al. (2018). New spin on organic radical batteries-an isoindoline nitroxide-based high-voltage cathode material. *ACS Applied Materials & Interfaces* 10 (9): 7982–7988.

195 Zhang, C., He, Y.W., Mu, P. et al. (2018). Toward high performance thiophene-containing conjugated microporous polymer anodes for lithium-ion batteries through structure design. *Advanced Functional Materials* 28 (4): 1705432.

196 Chen, G., Bai, Y., Gao, Y. et al. (2019). Inhibition of crystallization of poly(ethylene oxide) by ionic liquid: insight into plasticizing mechanism and application for solid-state sodium ion batteries. *ACS Applied Materials & Interfaces* 11 (46): 43252–43260.

197 Jinisha, B., Anilkumar, K.M., Manoj, M. et al. (2017). Poly (ethylene oxide) (PEO)-based, sodium ion-conducting, solid polymer electrolyte films, dispersed with Al_2O_3 filler, for applications in sodium ion cells. *Ionics* 24 (6): 1675–1683.

198 Li, S., Qiu, J.X., Lai, C. et al. (2015). Surface capacitive contributions: towards high rate anode materials for sodium ion batteries. *Nano Energy* 12: 224–230.

199 Liu, M.K., Zhang, P., Qu, Z.H. et al. (2019). Conductive carbon nanofiber interpenetrated graphene architecture for ultra-stable sodium ion battery. *Nature Communications* 10: 11.

200 Wang, Q.S., Yang, H., Meng, T. et al. (2021). Boosting electron transfer with heterointerface effect for high-performance lithium-ion storage. *Energy Storage Materials* 36: 365–375.

201 Wu, Z.Z., Xie, J., Xu, Z.C.J. et al. (2019). Recent progress in metal-organic polymers as promising electrodes for lithium/sodium rechargeable batteries. *Journal of Materials Chemistry A* 7 (9): 4259–4290.

202 Wu, S., Wang, W., Li, M. et al. (2016). Highly durable organic electrode for sodium-ion batteries via a stabilized alpha-c radical intermediate. *Nature Communications* 7: 13318.

203 Sun, T., Feng, X.L., Sun, Q.Q. et al. (2021). Solvation effect on the improved sodium storage performance of n-heteropentacenequinone for sodium-ion batteries. *Angewandte Chemie International Edition* 60 (51): 26806–26812.

204 Luo, C., Xu, G.L., Ji, X. et al. (2018). Reversible redox chemistry of azo compounds for sodium-ion batteries. *Angewandte Chemie International Edition* 57 (11): 2879–2883.

205 Tian, B.B., Zheng, J., Zhao, C.X. et al. (2019). Carbonyl-based polyimide and polyquinoneimide for potassium-ion batteries. *Journal of Materials Chemistry A* 7 (16): 9997–10003.

206 Liang, Y.J., Luo, C., Wang, F. et al. (2019). An organic anode for high temperature potassium-ion batteries. *Advanced Energy Materials* 9 (2): 1802986.

207 Kapaev, R.R., Zhidkov, I.S., Kurmaev, E.Z. et al. (2019). Hexaazatriphenylene-based polymer cathode for fast and stable lithium-, sodium- and potassium-ion batteries. *Journal of Materials Chemistry A* 7 (39): 22596–22603.

208 Wang, H.G., Yuan, S., Ma, D.L. et al. (2014). Tailored aromatic carbonyl derivative polyimides for high-power and long-cycle sodium-organic batteries. *Advanced Energy Materials* 4 (7): 1301651.

209 Pan, Z.H., Liu, X.M., Yang, J. et al. (2021). Aqueous rechargeable multivalent metal-ion batteries: advances and challenges. *Advanced Energy Materials* 11 (24): 2100608.

210 Qin, K.Q., Huang, J.H., Holguin, K. et al. (2020). Recent advances in developing organic electrode materials for multivalent rechargeable batteries. *Energy & Environmental Science* 13 (11): 3950–3992.

211 Zhu, J., Yao, M., Huang, S. et al. (2020). Thermal-gated polymer electrolytes for smart zinc-ion batteries. *Angewandte Chemie International Edition* 59 (38): 16480–16484.

212 Bin, D., Huo, W.C., Yuan, Y.B. et al. (2020). Organic-inorganic-induced polymer intercalation into layered composites for aqueous zinc-ion battery. *Chem* 6 (4): 968–984.

213 Shi, H.Y., Ye, Y.J., Liu, K. et al. (2018). A long-cycle-life self-doped polyaniline cathode for rechargeable aqueous zinc batteries. *Angewandte Chemie International Edition* 57 (50): 16359–16363.

214 Huang, J., Wang, Z., Hou, M. et al. (2018). Polyaniline-intercalated manganese dioxide nanolayers as a high-performance cathode material for an aqueous zinc-ion battery. *Nature Communications* 9 (1): 2906.

215 Wang, Y., Wang, C., Ni, Z. et al. (2020). Binding zinc ions by carboxyl groups from adjacent molecules toward long-life aqueous zinc-organic batteries. *Advanced Materials* 32 (16): 2000338.

216 Zhang, S., Zhao, W., Li, H. et al. (2020). Cross-conjugated polycatechol organic cathode for aqueous zinc-ion storage. *ChemSusChem* 13 (1): 188–195.

217 Dawut, G., Lu, Y., Miao, L.C. et al. (2018). High-performance rechargeable aqueous Zn-ion batteries with a poly(benzoquinonyl sulfide) cathode. *Inorganic Chemistry Frontiers* 5 (6): 1391–1396.

218 Lin, Z., Shi, H.Y., Lin, L. et al. (2021). A high capacity small molecule quinone cathode for rechargeable aqueous zinc-organic batteries. *Nature Communications* 12 (1): 4424.

219 Yoo, D.J., Heeney, M., Glocklhofer, F. et al. (2021). Tetradiketone macrocycle for divalent aluminium ion batteries. *Nature Communications* 12 (1): 2386.

220 Kim, D.J., Yoo, D.J., Otley, M.T. et al. (2018). Rechargeable aluminium organic batteries. *Nature Energy* 4 (1): 51–59.

221 Khayum, M.A., Ghosh, M., Vijayakumar, V. et al. (2019). Zinc ion interactions in a two-dimensional covalent organic framework based aqueous zinc ion battery. *Chemical Science* 10 (38): 8889–8894.

222 Wang, W., Kale, V.S., Cao, Z. et al. (2021). Molecular engineering of covalent organic framework cathodes for enhanced zinc-ion batteries. *Advanced Materials* 33 (39): 2103617.

223 Zhang, S.Q., Long, S.T., Li, H. et al. (2020). A high-capacity organic cathode based on active n atoms for aqueous zinc-ion batteries. *Chemical Engineering Journal* 400: 125898.

224 Tie, Z. and Niu, Z. (2020). Design strategies for high-performance aqueous Zn/organic batteries. *Angewandte Chemie International Edition* 59 (48): 21293–21303.

225 Zhang, H., Xie, S.J., Cao, Z.Y. et al. (2021). Extended π-conjugated system in organic cathode with active C=N bonds for driving aqueous zinc-ion batteries. *ACS Applied Energy Materials* 4 (1): 655–661.

226 Ye, Z.L., Xie, S.J., Cao, Z.Y. et al. (2021). High-rate aqueous zinc-organic battery achieved by lowering HOMO/LUMO of organic cathode. *Energy Storage Materials* 37: 378–386.

227 Wang, W.X., Kale, V.S., Cao, Z. et al. (2020). Phenanthroline covalent organic framework electrodes for high-performance zinc-ion supercapattery. *ACS Energy Letters* 5 (7): 2256–2264.

228 Luo, C., Wang, J.J., Fan, X.L. et al. (2015). Roll-to-roll fabrication of organic nanorod electrodes for sodium ion batteries. *Nano Energy* 13: 537–545.

229 Gao, Y.J., Li, G.F., Wang, F. et al. (2021). A high-performance aqueous rechargeable zinc battery based on organic cathode integrating quinone and pyrazine. *Energy Storage Materials* 40: 31–40.

230 Yang, X., Hu, Y., Dunlap, N. et al. (2020). A truxenone-based covalent organic framework as an all-solid-state lithium-ion battery cathode with high capacity. *Angewandte Chemie International Edition* 59 (46): 20385–20389.

231 Shehab, M.K., Weeraratne, K.S., Huang, T. et al. (2021). Exceptional sodium-ion storage by an aza-covalent organic framework for high energy and power density sodium-ion batteries. *ACS Applied Materials & Interfaces* 13 (13): 15083–15091.

232 Wang, Z., Li, Y., Liu, P. et al. (2019). Few layer covalent organic frameworks with graphene sheets as cathode materials for lithium-ion batteries. *Nanoscale* 11 (12): 5330–5335.

233 Wu, X.Y., Ma, J., Ma, Q.D. et al. (2015). A spray drying approach for the synthesis of a $Na_2C_6H_2O_4$/CNT nanocomposite anode for sodium-ion batteries. *Journal of Materials Chemistry A* 3 (25): 13193–13197.

234 Wu, Z.Z., Adekoya, D., Huang, X. et al. (2020). Highly conductive two-dimensional (2D) metal-organic framework (MOFs) for resilient lithium storage with superb rate capability. *ACS Nano* 14: 12016–12026.

235 Yang, K., Liu, Q.R., Zheng, Y.P. et al. (2021). Locally ordered graphitized carbon cathodes for high-capacity dual-ion batteries. *Angewandte Chemie International Edition* 60 (12): 6326–6332.

236 Speer, M.E., Kolek, M., Jassoy, J.J. et al. (2015). Thianthrene-functionalized polynorbornenes as high-voltage materials for organic cathode-based dual-ion batteries. *Chemical Communications* 51 (83): 15261–15264.

237 Dong, S.Y., Li, Z.F., Rodríguez-Pérez, I.A. et al. (2017). A novel coronene//Na$_2$Ti$_3$O$_7$ dual-ion battery. *Nano Energy* 40: 233–239.

238 Deunf, É., Moreau, P., Quarez, É. et al. (2016). Reversible anion intercalation in a layered aromatic amine: a high-voltage host structure for organic batteries. *Journal of Materials Chemistry A* 4 (16): 6131–6139.